ENERGY CONFINEMENT IN THE TOKAMAK DEVICES PULSATOR AND ASDEX

O.Klüber and H.Murmann

IPP III/72 April 1982

MAX-PLANCK-INSTITUT FÜR PLASMAPHYSIK

8046 GARCHING BEI MÜNCHEN

MAX-PLANCK-INSTITUT FÜR PLASMAPHYSIK

GARCHING BEI MÜNCHEN

ENERGY CONFINEMENT IN THE TOKAMAK DEVICES PULSATOR AND ASDEX

O.Klüber and H.Murmann

IPP III/72 April 1982

Die nachstehende Arbeit wurde im Rahmen des Vertrages zwischen dem Max-Planck-Institut für Plasmaphysik und der Europäischen Atomgemeinschaft über die Zusammenarbeit auf dem Gebiete der Plasmaphysik durchgeführt.

IPP III/72

O.Klüber
H.Murmann

ENERGY CONFINEMENT IN THE TOKAMAK DEVICES PULSATOR AND ASDEX

April 1982

Abstract

The energy confinement of ohmically heated hydrogen plasmas obtained in the ASDEX and Pulsator tokamaks is investigated. In both devices, the confinement time does not follow a simple scaling law of the type $\tau_E \propto n_e a^2$. In the case of Pulsator, a regime is identified in which the transport is governed by electron heat conduction. The experimental data are compared with an analytic solution of the energy balance equation from which a heat diffusivity $\chi_e \propto Z_{eff}^{1/3}/n_e(r)T_e^{1/2}(r)q(r)$ is inferred. χ_i is supposed to be neoclassical (plateau regime). Heat conduction following these laws is shown to lead to a consistent description of the full data set.

CONTENTS

1. INTRODUCTION

In this paper, the energy confinement times of ohmically heated hydrogen plasmas obtained in the ASDEX and Pulsator tokamak devices are compared. For both machines the maximum toroidal magnetic field is nearly the same, namely 27 - 28 kG. ASDEX is an axisymmetric divertor tokamak, the separatrix of which is nearly circular. Experiments using a material limiter indicate that neither the shapes of the density and temperature profiles nor the values of the energy confinement times are different for the two modes of operation under otherwise equal conditions. Thus, with respect to confinement behaviour, the most important difference between the machines is their size: the ratio of the plasma cross-sections is 13.

It should be pointed out that in both experiments the study of confinement was not a major aim of the investigation. Systematic parameter studies, in particular large variations of the toroidal magnetic field, were not performed. Nevertheless, a lot of data are available which clearly show that in both machines the energy confinement time can be described at low densities by a simple scaling law of the type

$$\tau_E = c_n \bar{n}_e a^2 \quad , \tag{1}$$

where a is the minor radius of the plasma column and c_n is a constant. At elevated density, however, τ_E tends to saturate. This might be due to the contribution of the ions to the energy balance since the increasing density leads to enhanced coupling between the electrons and the ions. Under the experimental conditions realized in the ASDEX and Pulsator devices, the ions are in the plateau regime, as is the case for practically all tokamaks which are purely ohmically heated. The ion heat

conductivity $\kappa_i = n_i \chi_i$ thus grows with n_i and with the ion temperature as $T_i^{3/2}$. It is conceivable, therefore, that the total energy confinement time saturates, while that of the electron component continues to increase with density.

This paper is mainly aimed at studying these questions as quantitatively as the experimental data allow. Hence the energy balance equations

$$\frac{3}{2}\frac{\partial}{\partial t}(n_e k T_e) - \frac{1}{r}\frac{\partial}{\partial r} r\left(n_e \chi_e \frac{\partial k T_e}{\partial r} - \frac{3}{2} n_e k T_e v_r\right) = j_\varphi E_\varphi - p_{ei} - p_{rad} \quad ; \tag{2}$$

$$\frac{3}{2}\frac{\partial}{\partial t}(n_i k T_i) - \frac{1}{r}\frac{\partial}{\partial r} r\left(n_i \chi_i \frac{\partial k T_i}{\partial r} - \frac{3}{2} n_i k T_i v_r\right) = p_{ei} - p_{cx} \tag{3}$$

of the electrons and ions have to be discussed. Here j_φ and E_φ are the toroidal current density and electric field, respectively; in the following, the index φ will be omitted. The power density transferred from the electrons to the ions is given by

$$p_{ei} = 3\frac{m_e}{m_i}\frac{n_e k (T_e - T_i)}{\tau_{ei}} = \frac{6 (e n_e)^2}{m_i \sigma_{Sp}} k (T_e - T_i) \tag{4}$$

where τ_{ei} is the inverse electron-ion collision frequency and σ_{sp} the Spitzer conductivity, p_{rad} and p_{cx} denote the power loss densities due to radiation and charge exchange, respectively, and v_r is the radial component of the mass velocity, the notation of the other quantities being standard.

In the next section it will be shown that the ASDEX and Pulsator plasmas can be considered to be stationary or quasi-stationary,

which means that the temporal derivatives in eqs. (2) and (3) can be set equal to zero, and the toroidal electric field E is uniform apart from the 1/R dependence not considered here since eqs. (2) and (3) are based on the cylindrical approximation. Furthermore, it is shown that except from the near-boundary region p_{rad} and p_{cx} are negligible. Thus, eqs. (2) and (3) can be reduced to

$$-\frac{1}{r}\frac{\partial}{\partial r} r\left(n_e \chi_e \frac{\partial kT_e}{\partial r} - \frac{3}{2} n_e kT_e v_r\right) = jE - p_{ei} \quad ; \tag{2a}$$

$$-\frac{1}{r}\frac{\partial}{\partial r} r\left(n_i \chi_i \frac{\partial kT_i}{\partial r} - \frac{3}{2} n_i kT_i v_r\right) = p_{ei} \quad . \tag{3a}$$

In Section 2 the parameter range is also described, e.g. that of the safety factor

$$q_a = \frac{aB_\varphi}{RB_a} = \frac{2\pi a^2 B_\varphi}{\mu_o R \cdot I} \tag{5}$$

the notation being standard.

The remainder of the paper is organized as follows: Section 3 discusses the profiles of the electron and ion temperatures and of the electron density. From these profiles the quasi-local confinement times $\tau_{Ee}(r)$ and $\tau_{Ei}(r)$ can be obtained by integrating eqs. (2a) and (3a) over the radius:

$$-2\pi r\left(n_e \chi_e \frac{\partial kT_e}{\partial r} - \frac{3}{2} n_e kT_e v_r\right) \equiv \frac{3}{2}\frac{1}{\tau_{Ee}(r)} \int_0^r n_e kT_e \cdot 2\pi r' dr' = E \cdot I(r) - P_{ei} \quad ; \tag{2b}$$

$$-2\pi r\left(n_i \chi_i \frac{\partial kT_i}{\partial r} - \frac{3}{2} n_i kT_i v_r\right) \equiv \frac{3}{2} \frac{1}{\tau_{Ei}(r)} \int_0^r n_i kT_i \cdot 2\pi r' dr' = P_{ei} \tag{3b}$$

where

$$I(r) = 2\pi \int_0^r j(r') r' dr' \tag{6}$$

is the current flowing inside the magnetic surface with the radius r, and where

$$P_{ei}(r) = 2\pi \int_0^r p_{ei}(r') r' dr' \quad . \tag{4b}$$

At elevated density, the problem arises as to how to determine the difference $EI(r) - P_{ei}(r)$ with sufficient accuracy. For this reason the total energy confinement time $\tau_E(r)$ is introduced, this being defined by adding eqs.(2b) and (3b):

$$\frac{3}{2} \frac{1}{\tau_{Ee}(r)} \int_0^r n_e kT_e \cdot 2\pi r' dr' + \frac{3}{2} \frac{1}{\tau_{Ei}(r)} \int_0^r n_i kT_i \cdot 2\pi r' dr' \equiv$$

$$\equiv \frac{3}{2} \frac{1}{\tau_E(r)} \int_0^r (n_e kT_e + n_i kT_i) 2\pi r' dr' = E \cdot I(r) \quad . \tag{7}$$

The radial dependence of the energy confinement time and the contribution of the particle flow with the velocity v_r to the energy transport are discussed in Section 3. Section 4 is dedicated to a study of the parameter dependence of $\tau_E \equiv \tau_E(a)$ and $\tau_{Ee} \equiv \tau_{Ee}(a)$ and of $\{T_s\}$, the particle-averaged value of $T_e + T_i$; empirical formulas describing these quantities

are derived. The influence of the sawtooth relaxations on the profiles and on the energy losses is investigated in Section 5.

The interpretation of the results is given in Section 6. The ion thermal conductivity is supposed to be neoclassical (plateau regime) and to be described by the Galeev-Sagdeev formula /1/. For the electron thermal conductivity, a semi-empirical formula is established following a procedure proposed by Guest, Miller, Pfeiffer and Waltz /2/. It is shown that these two formulas are capable of explaining the experimental findings. The essential results are summarized in Section 7.

2. PARAMETER RANGE AND DISCHARGE CONDITIONS

The characteristic data of both machines are given in Table 1. The experimental conditions under which the confinement behaviour was investigated can be described as follows:
In the Pulsator device, the majority of the discharges were performed at the maximum toroidal field of 2.7 T; in addition, a smaller number of shots at $B_\varphi = 2.1$ T were investigated. At both B_φ values, the plasma current was varied so that the range $2.7 \leq q_a \leq 5.4$ was covered; this means 45 kA $\leq I \leq$ 9o kA at 2.7 and 35 kA $\leq I \leq$ 7o kA at 2.1 T.
This paper treats the ASDEX data obtained in the first year of operation. In this period, the machine has nearly always been operated at $B_\varphi = 2.2$ T, and for this value usually with a plasma current of 24o kA, resulting in $q_a = 4.4$. Some data were obtained at slightly different currents corresponding to $4.3 < q_a < 4.7$ and a few profiles were taken at $B_\varphi = 1.9$ T, I = 41o kA. Thus an eventual dependence of the confinement on the toroidal magnetic field can hardly be obtained from both the Pulsator and ASDEX data.

Table 1

ASDEX and Pulsator data

	ASDEX	Pulsator	Ratio
Major radius R	165 cm	70 cm	2.36
Minor radius a	40 cm	11 cm	3.64
Aspect ratio A	4.13	6.36	0.65
Plasma cross section πa^2	5027 cm^2	380 cm^2	13.2
Plasma volume	$5.21 \times 10^6 cm^3$	$0.17 \times 10^6 cm^3$	31.2
Max.toroidal field $B_\varphi^{(max)}$	2.8 T	2.7 T	1.04
Plasma current at $B_\varphi^{(max)}$ and $q_a=4$	340 kA	58 kA	5.86
Pulse duration	3 s	0.1 s	30

The temporal evolution of the plasma current I, the loop voltage U_l, the mean electron density $\bar{n}_e$ and the Z_{eff} value in a typical ASDEX discharge are shown in Fig. 1. Here and in the following, $\bar{n}_e$ denotes the line-averaged density

$$\bar{n}_e = \frac{1}{a} \int_0^a n_e(r)\, dr$$

which is measured by interferometry (2 mm and 0.3 mm). The I(t) curve is controlled by a feedback system which allows a preprogrammed function to be followed. Precise current plateaus can thus be produced, which means that the loop voltage is purely resistive and the toroidal electric field is uniform over the plasma cross-section (apart from the 1/R dependence), provided that the current density profile j (r)

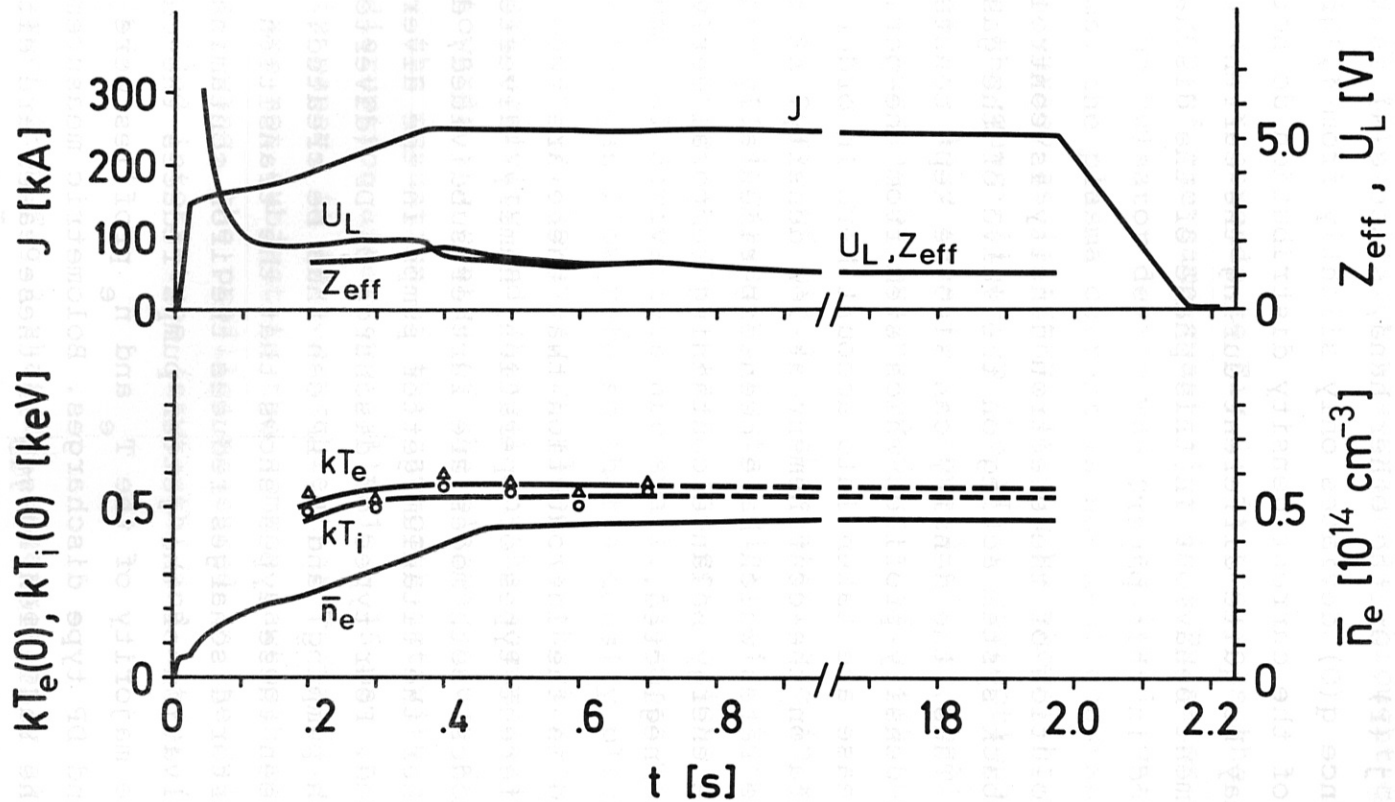

Fig. 1: A typical ASDEX discharge.
Above: Plasma current I, loop voltage U_L and effective ion charge Z_{eff}.
Below: Line-averaged electron density $\bar{n}_e$, central electron and ion temperatures $T_e(0)$ and $T_i(0)$.

does not change. Actually, in almost all cases the well-known sawtooth activity is observed during the current flat-top indicating a periodic but rather small modulation of the current density profile j (r). On the other hand, since q(a) is kept constant and since q(O) deviates only slightly from 1, gross rearrangements of the current density distribution do not occur. The situation may be quite different during the current rise, but the confinement behaviour in this phase of the discharge is not considered in this paper.

The temporal evolution of the electron density is controlled by another feedback system acting on the valve of the gas feed equipment. Thus, the density can also be kept constant. Temperature and density profiles which stem from the period of density increase are taken into account here in order to achieve more data on the confinement at low density. At the density increase rates which have been experimentally realized the terms of the energy balance containing temporal derivatives of n or T can be neglected.

It was mentioned in the introduction that there are two essentially different types of operation, namely "divertor" and "limiter" modes. Both modes are further subdivided, depending on whether the titanium getter pumps in the divertor chambers are used. Four types of discharge D, DP (divertor without and with pumping) and L, LP can thus be created. A comparison between these types shows that the transition from limiter to divertor discharges reduces the iron contamination, whereas the activation of the getter pumps reduces the oxygen content /3/. The majority of the T_e and n_e profiles were recorded in D and DP type discharges. Bolometric measurements /4/ show that the radiation losses in these cases are either small as compared with the ohmic power input, or that

the power is radiated from regions near the boundary and hence from regions which contribute very little to the energy content, and where almost no heating occurs. This also holds for the so-called LD type discharges, in which the retractable limiter was gradually brought closer to the separatrix.

Figure 2 corresponds to Fig.1: it presents the temporal evolution of the same quantities in a Pulsator discharge. Since the Pulsator device was not equipped with feedback-systems, the plasma current is not kept constant with the same accuracy as in ASDEX. It can be shown, however, that during the quasi-flat-top the $\partial I/\partial t$ corrections of the loop voltage are less than 1o %; thus $\partial E/\partial r$ is small and the OH power input can be evaluated with sufficient accuracy.

The $\bar{n}_e(t)$ curve of Fig.2 is characteristic in that the density continues to increase up to the disruptive termination of the discharge. In most cases, the corrections of τ_E due to the temporal derivatives are small. Attempts were made to change the gas flow rate so that a density plateau was achieved. These attempts, however, resulted in the termination of the sawtooth activity and (hence) in the accumulation of impurities towards the centre of the plasma column /5,6/. In all cases, the cessation of the sawtooth activity is followed by a disruption after typically 1o - 15 ms. In the context, of this paper, it is remarkable that T_e profiles can be achieved which are not subject to the common sawtooth modulation. In the following, the profiles measured in the Pulsator device are divided into S-type (sawteeth) and A-type (accumulation) profiles.

It is seen from Fig.2 that Z_{eff} changes only slightly with time, i.e. with $\bar{n}_e$. This behaviour is typical of the discharges obtained in the last two years of Pulsator operation,

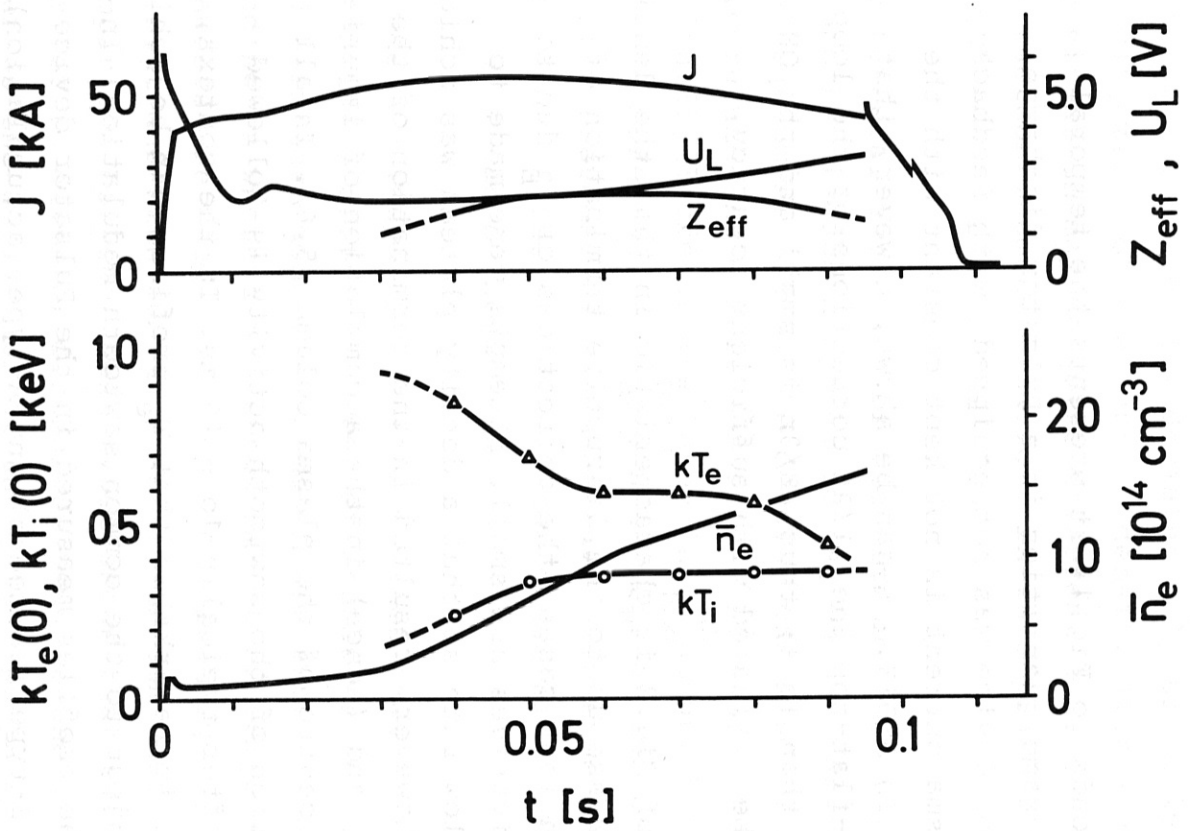

Fig. 2: A typical Pulsator discharge.
Above: Plasma current I, loop voltage U_L and effective ion charge Z_{eff}.
Below: Line-averaged electron density $\bar{n}_e$, central electron and ion temperatures $T_e(0)$ and $T_i(0)$.

it is shown in Fig.3. At the very beginning of the high-density operation phase, the Z_{eff} values obtained just before the start of the gas input amounted to 6 - 8 and dropped to ~2 during the density rise /7/. Data from the beginning of the high-density performance are not considered in this paper for the following reasons:

- There are only a few measurements of the ion temperature during this period.

- Most likely the radiation losses from the central region due to the emission of Fe and Mo lines cannot be neglected in the case of the discharges starting with Z_{eff} as large as 6 - 8. Since there were no bolometer measurements at this time, these discharges are ruled out.

At the end of the Pulsator operation period a bolometer was installed. The radiation losses were found to amount to up to 6o % of the power input and to arise from the outermost zones of the plasma /8/. The predominant impurity appears to be oxygen. Thus the radiation losses are negligible for radii <8 cm.

The same holds for the energy losses due to charge exchange in Pulsator discharges. The investigation of the energy balance of the ions based on the analysis of the charge exchange flux /9/ shows that P_{cx} is important in the central regions only at very low densities, at which the contribution of the ions to the energy balance of the plasma becomes negligible. In the case of ASDEX, charge exchange is expected to be negligible at even smaller densities because the critical quantity is na.

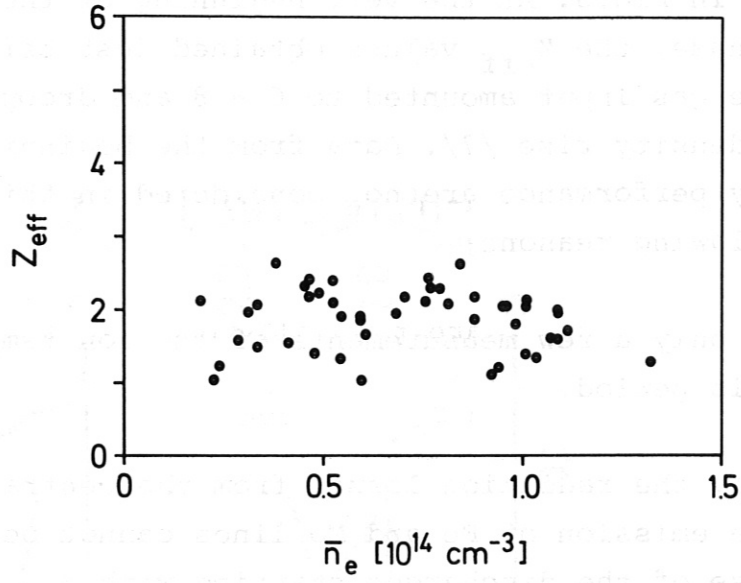

Fig. 3: Pulsator.
Z_{eff} versus $\bar{n}_e$. Apparently, there is no correlation between Z_{eff} and the density.

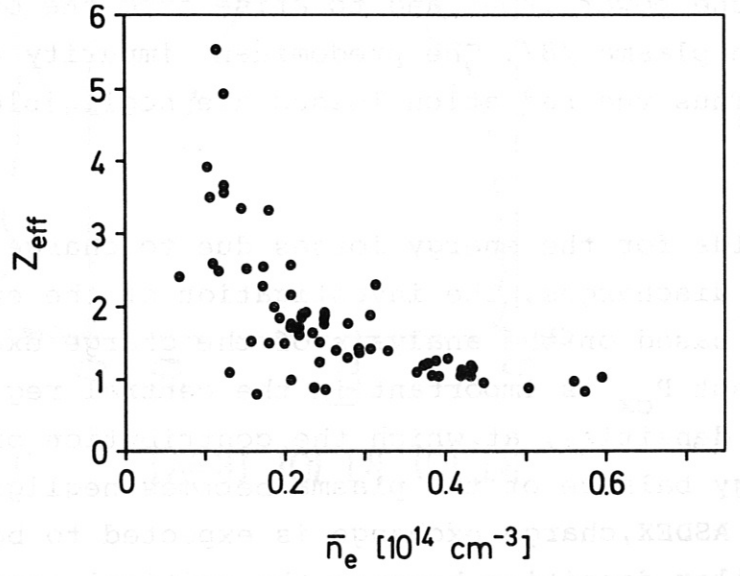

Fig. 4: ASDEX.
Z_{eff} versus $\bar{n}_e$. At low density, $Z_{eff} \sim 1$ can be achieved in DP-type plasmas, whereas large values of Z_{eff} are obtained in L-type and unconditioned D-type discharges.

Thus, the energy balance equations (2) and (3) can be appreciably simplified by ignoring the temporal derivatives and the terms P_{rad} and P_{cx}. They then read

$$-\frac{1}{r}\frac{\partial}{\partial r} r\left(n_e \chi_e \frac{\partial kT_e}{\partial r} - \frac{3}{2} n_e kT_e v_r\right) = j(r)E - p_{ei} \quad ; \tag{2a}$$

$$-\frac{1}{r}\frac{\partial}{\partial r} r\left(n_i \chi_i \frac{\partial kT_i}{\partial r} - \frac{3}{2} n_i kT_i v_r\right) = p_{ei} \quad . \tag{3a}$$

It is seen from Fig. 2 that the central electron temperature $T_e(0)$ decreases with time, i.e. with increasing density. This behaviour is typical of Pulsator discharges as can be seen from Fig. 5, where $T_e(0)$ is plotted versus $\bar{n}_e$. Obviously, this behaviour is not due to a decrease of Z_{eff} since it was shown above that there is no systematic dependence of Z_{eff} on the density (see Fig.3).

In the case of ASDEX the situation is somewhat different. From the Z_{eff} versus $\bar{n}_e$ plot (Fig.4) it is seen that Z_{eff} is close to unity at the upper end of the $\bar{n}_e$ range, whereas the "bandwidth" becomes broader with decreasing density. The discharges with larger values of Z_{eff} are those with a material limiter or D type discharges obtained in unconditioned states of the machine. In the $T_e(0)$ versus $\bar{n}_e$ plot (Fig.6) different symbols are used, depending on whether $Z_{eff} > 1.3$ or $Z_{eff} < 1.3$. It is demonstrated in this way that the larger values of $T_e(0)$ obtained at low densities are primarily due to the larger Z_{eff}, whereas the central electron temperature varies only slightly if discharges with $Z_{eff} \sim 1$ are considered.

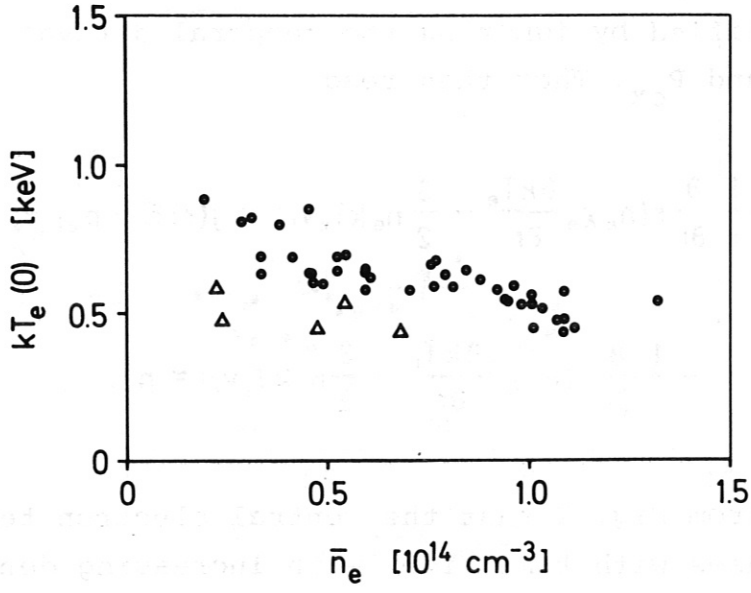

Fig. 5: Pulsator.
The central electron temperature versus $\bar{n}_e$.
O: $B_\varphi = 27$ kG; Δ: $B_\varphi = 21$ kG.

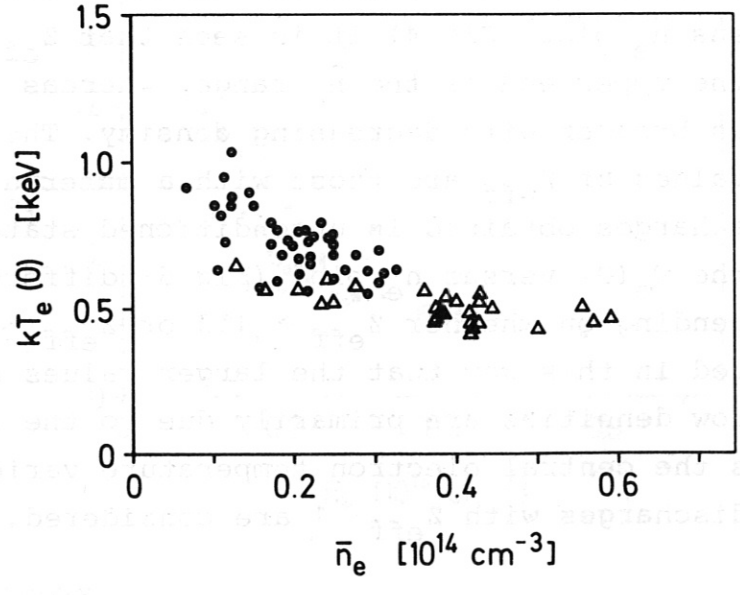

Fig. 6: ASDEX.
The central electron temperature versus $\bar{n}_e$.
O: $Z_{eff} > 1.3$; Δ: $Z_{eff} \leq 1.3$.

Finally, Figs. 1 and 2 are typical examples of the density dependence of the central ion temperature: While $T_i(0) \ll T_e(0)$ at low and $T_i(0) \sim T_e(0)$ at high density in the case of Pulsator, both temperatures are nearly equal at all densities in ASDEX discharges. In Figs. 7 and 8 the ratio $T_e(0)/T_i(0)$ is plotted versus $\bar{n}_e$ for Pulsator and ASDEX, respectively. The approach of the temperatures at the largest densities in both machines is quite obvious since the power transferred from the electrons to the ions cannot exceed the ohmic heating power. The consequences can be discussed quantitatively by comparing the central values $p_{ei}(0)$ and $p_{OH}(0) = j(0)E$. With eq. (4) and with

$$E = \frac{j(r)}{\sigma(r)} = \frac{j(o)}{\sigma(o)} = \frac{2 B_\varphi Z_{eff}}{\mu_0 R q(o) \sigma_{Sp}(o)} \tag{8}$$

we get for $q(0) = 1$

$$\frac{p_{ei}(o)}{p_{OH}(o)} = \frac{3}{2 Z_{eff} m_i} \left(\frac{e n_e(o) \mu_0 R}{B_\varphi}\right)^2 k\left(T_e(o) - T_i(o)\right) \quad . \tag{9}$$

Let $(\Delta kT(0))_{1/2}$ be the value of the difference $kT_e(0) - kT_i(0)$, which leads to $p_{ei}(0) = p_{OH}(0)/2$. According to eq. (9), $(\Delta kT(0))_{1/2}$ depends quadratically on $n_e(0)R/B_\varphi$. In Fig. 9, this quantity is plotted versus $\bar{n}_e$ instead of $n_e(0)$, where $\bar{n}_e = 2n_e(0)/3$ is assumed. For ASDEX and Pulsator the typical data $B_\varphi = 2.2$ T, $Z_{eff} = 1.5$ and $B_\varphi = 2.7$ T, $Z_{eff} = 2$ are chosen, respectively. It is seen from this figure that for ASDEX $(\Delta kT(0))_{1/2} < 40$ eV if $\bar{n}_e > 5 \times 10^{13}$ cm^{-3}. Hence at these densities the difference of the actual central temperatures cannot exceed 80 eV and the values of $T_e(0)/T_i(0)$ close to 2 shown in Fig.8 must be ascribed to errors.

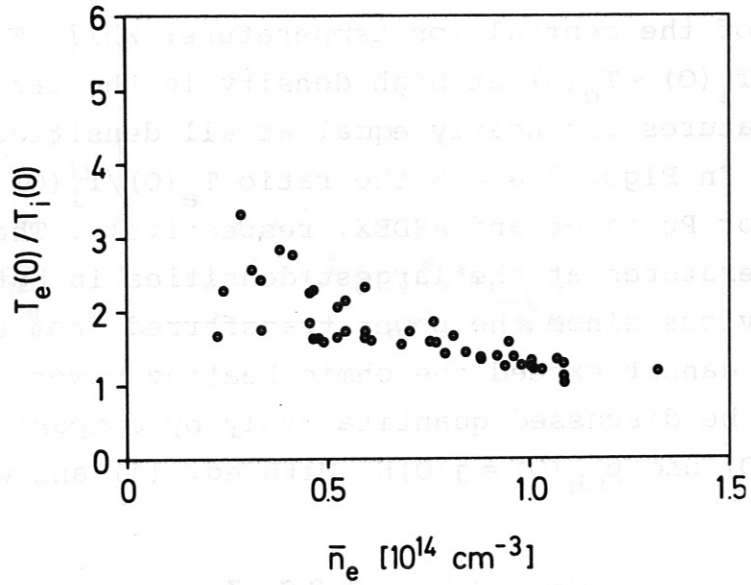

Fig. 7: Pulsator.
The ratio of the central electron and ion temperatures versus $\bar{n}_e$.

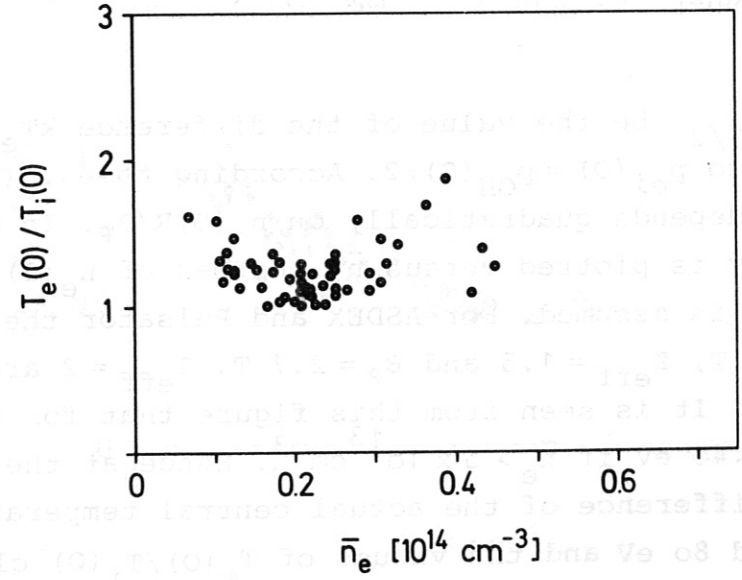

Fig. 8: ASDEX.
The ratio of the central electron and ion temperatures versus $\bar{n}_e$.

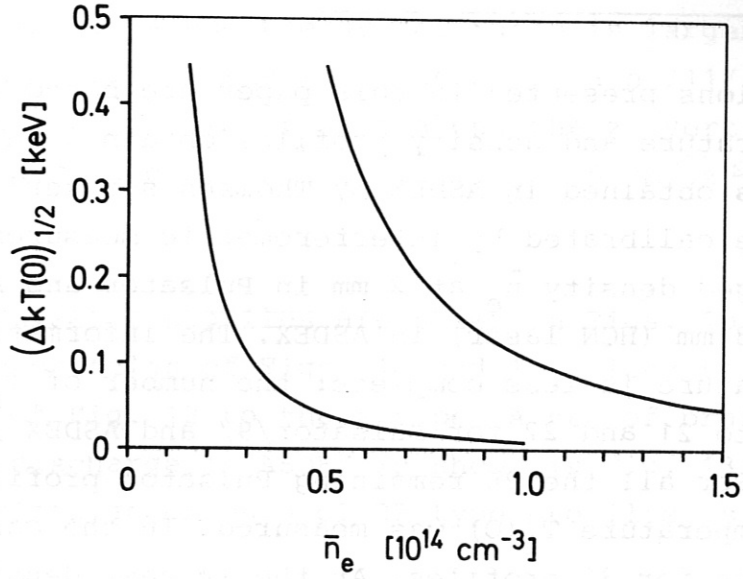

Fig. 9: $(\Delta kT(O))_{1/2}$, the difference of the central temperatures needed to transfer half of the central ohmic heating power to the ions, versus $\bar{n}_e$. Left-hand curve: ASDEX: 22 kG. Right-hand curve: Pulsator: 27 kG.

3. TEMPERATURE AND DENSITY PROFILES

The investigations presented in this paper are based on 47 electron temperature and density profiles obtained in Pulsator and 7o profiles obtained in ASDEX by Thomson scattering. The n_e profiles are calibrated by interferometric measurements of the line-averaged density $\bar{n}_e$ at 2 mm in Pulsator and ASDEX, and also at 0.3 mm (HCN laser) in ASDEX. The information on the ion temperature is less complete: the number of T_i profiles amounts to 21 and 22 for Pulsator/9/ and ASDEX /1o/, respectively. For all the 26 remaining Pulsator profiles, the central ion temperature $T_i(0)$ was measured. In the case of ASDEX this holds for 32 profiles. At the largest densities obtained in the ASDEX device the charge-exchange flux diminishes drastically and therefore does not allow determination of the central ion temperature. At these densities, however, the ion temperature is necessarily close to the electron temperature according to the considerations presented above.

In both machines the Thomson scattering laser beam passes vertically through the torus. In the Pulsator device, the plasma is usually scanned in the midplane. Let x denote the coordinate in the direction of the major radius, $x = 0$ the centre of the plasma column, and $x > 0$ the outside of the torus. The accessible region is $-4\ \text{cm} < x < 8\ \text{cm}$. The Thomson scattering systems delivers one point per shot. In the ASDEX device the laser beam cannot be displaced horizontally owing to the presence of the multipole triplets; it passes the midplane of the torus at the fixed position $x = -1$ cm, and hence somewhat apart from the magnetic axis. In the ASDEX discharges treated in this paper the equilibrium parameter $\Lambda = \beta_p + l_i/2$ does not exceed 1; in this case the magnetic axis is located at $x = 4$ cm, which means a displacement by 1o % of the minor radius (the

same relative displacement is reached in the Pulsator device if $\beta_p + l_i/2$ is 1.5 since the aspect ratio is larger). The ASDEX detection system in the setup used to date /11/ allows 1o spatial points per laser shot along the z (vertical) axis; they are arranged so that the region $-15\ cm \leq z \leq 3o\ cm$ is covered.

Typical Pulsator profiles are shown in Figs. 1o, 11 and 12, where the profiles of Figs. 1o and 11 belong to the S-type and that of Fig. 12 to the A-type. A set of profiles from a D-type discharge in ASDEX is shown in Fig. 13; for the sake of comparison an example of DP type profiles is shown in Fig. 14.

It is seen from these figures that the particular properties of the machines and of the different discharge types obtained in them do not influence the general character of the profiles:

The electron temperature profiles are bell-shaped; their width is smaller the larger the q value at the boundary is. In the preceding section it was shown that the electric field can be considered to be uniform. If, in addition, Z_{eff} is assumed to be independent of the radius, the profiles of the current density j (r) and of

$$q(r) = \frac{2\pi r^2 B_\varphi}{\mu_0 R \cdot I(r)} \qquad (1o)$$

can be calculated. In the case of Pulsator profiles the q(O) values amount typically to 0.8 - 1.2 for both S-type and A-type discharges if the corrections due to trapped electrons are neglected. This result indicates that Z_{eff} is nearly uniform in Pulsator plasmas.

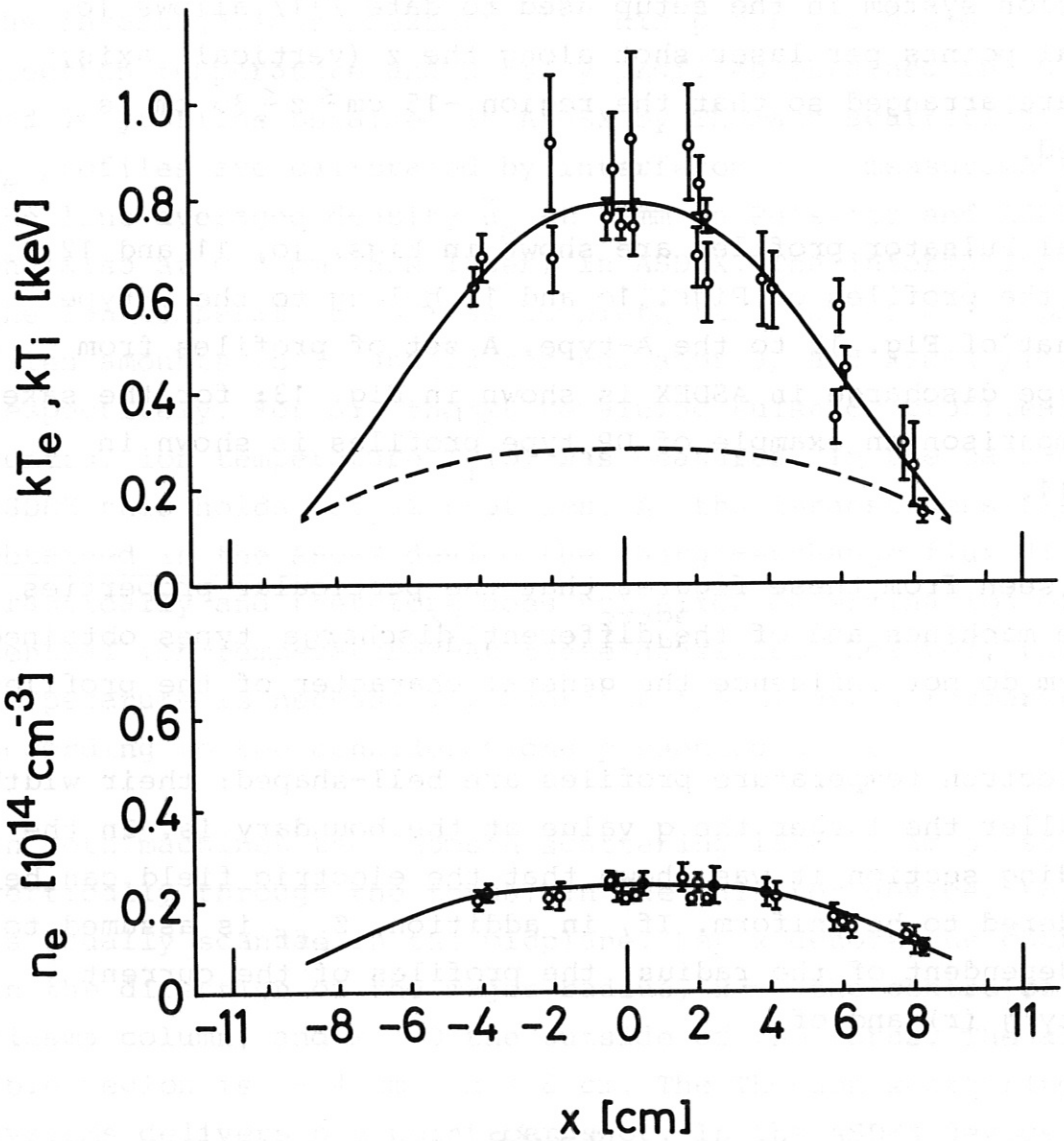

Fig.1o: Pulsator.
Profiles of electron temperature (———), ion temperature (-----) and electron density for an S-type discharge.

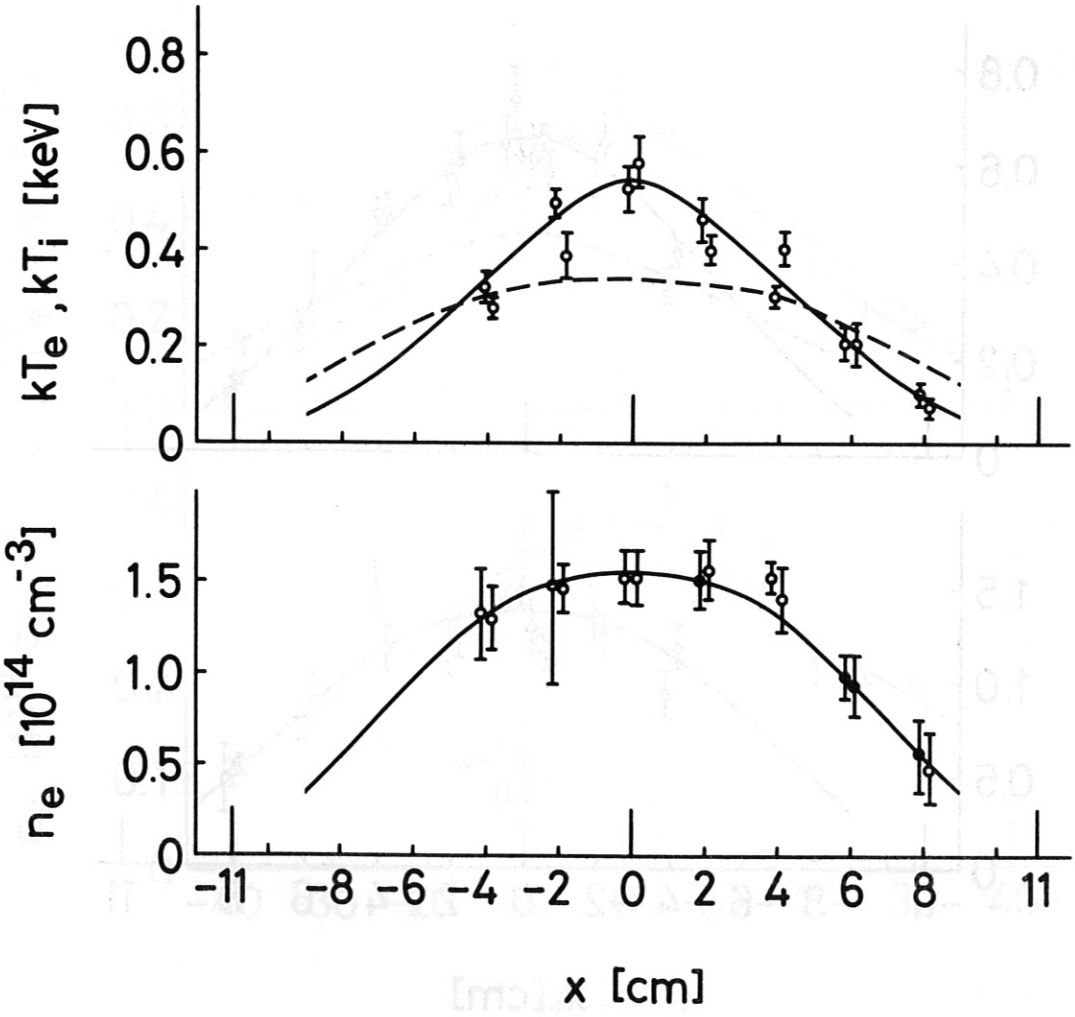

Fig.11: Pulsator.
Profiles of electron temperature (———), ion temperature (-----) and electron density for an S-type discharge.

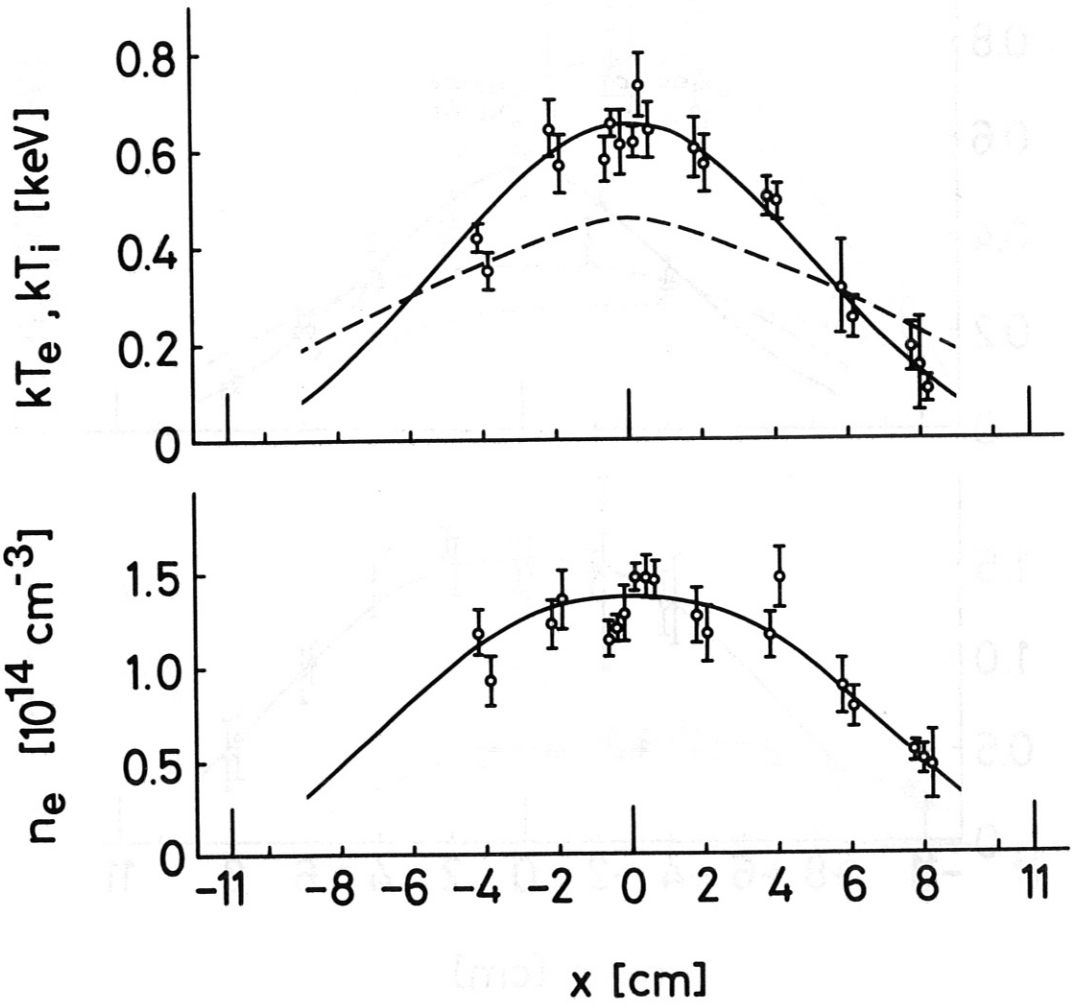

Fig.12: Pulsator.
Profiles of electron temperature (———), ion temperature (-----) and electron density for an A-type discharge.

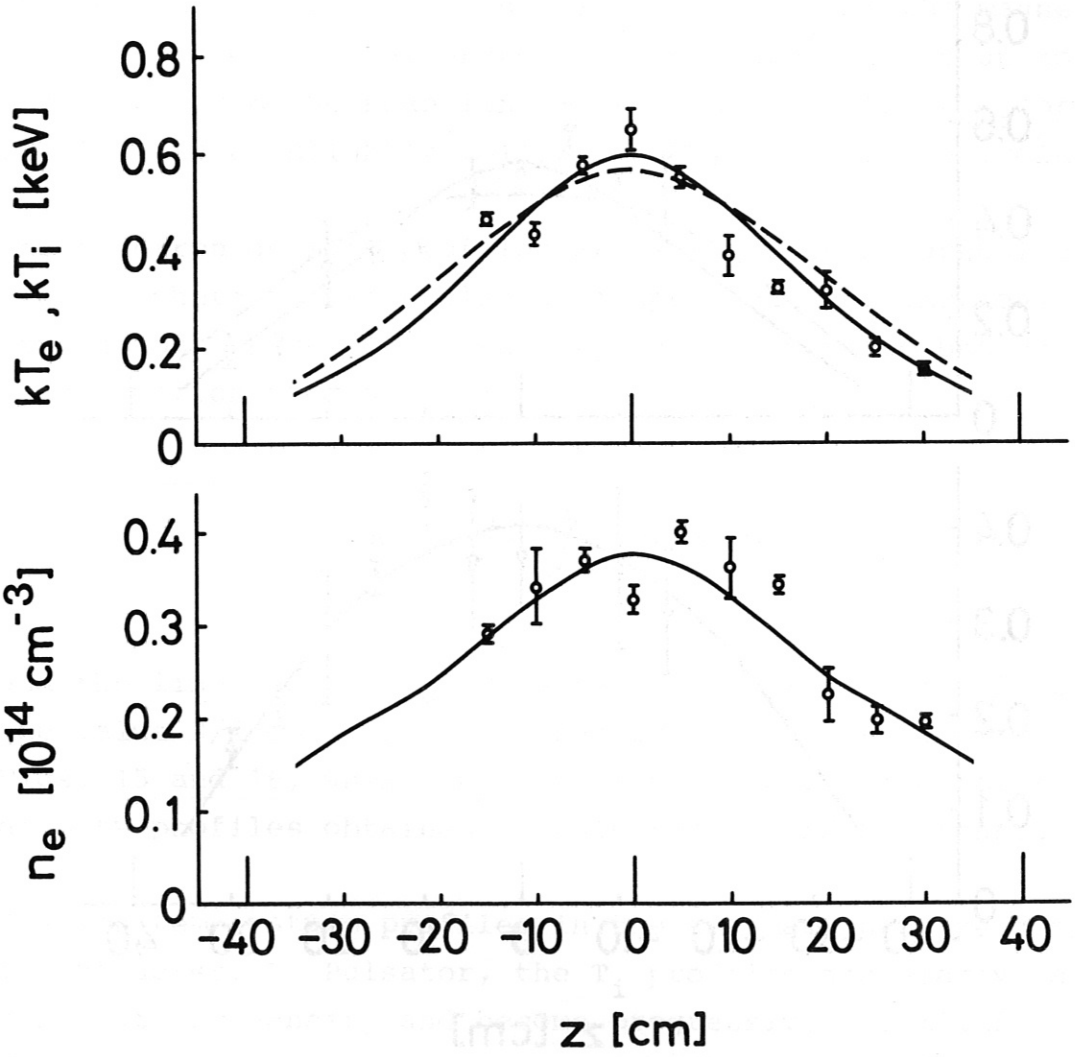

Fig.13: ASDEX.
Profiles of electron temperature (———), ion temperature (-----) and electron density for a D-type discharge.

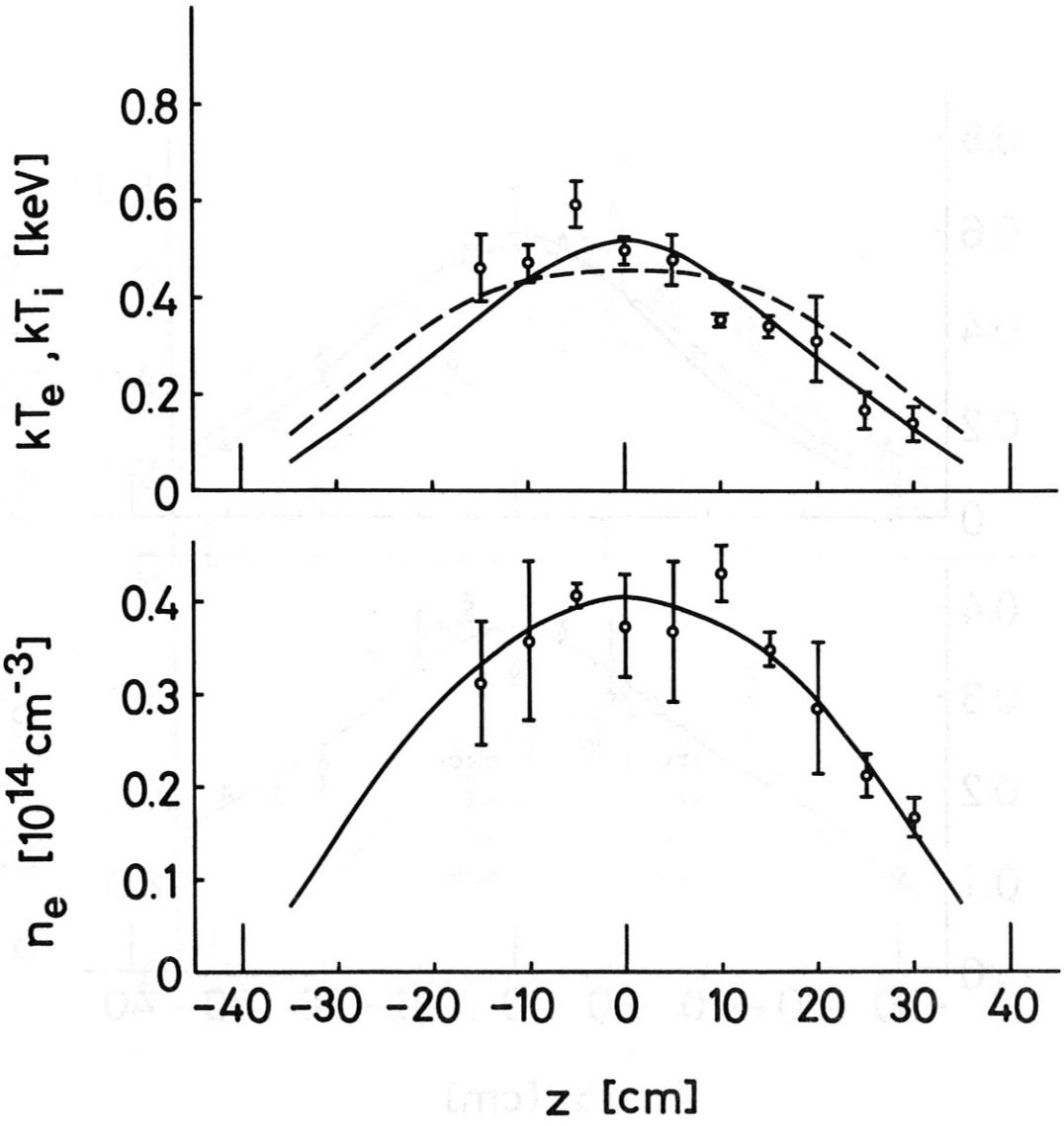

Fig.14: ASDEX.
Profiles of electron temperature (———), ion temperature (-----) and electron density for a DP-type discharge.

In the case of ASDEX, profiles leading to $q(0) < 1$ are rare; for the majority of profiles one gets $q(0) = 1.2 \pm 0.1$, which is in contrast to the experimentally observed occurrence of sawtooth relaxations. This discrepancy might be partly due to the geometry of the Thomson scattering system: the magnetic axis and hence the temperature maximum are located up to 5 cm away from the scan line. A tendency for the Z_{eff} profiles in ASDEX to be slightly hollow cannot, however, be excluded.

The electron density profiles are more or less parabolic; even if there is triangular or trapezoidal deformation, they remain quasi-parabolic with respect to the ratio between the cross-section-averaged value

$$\langle n_e \rangle = \frac{1}{\pi a^2} \int_0^a n_e(r') \, 2 \pi r' \, dr'$$

and the line average $\bar{n}_e$. This ratio is always very close to the value 3/4 obtained for a parabola. This is seen from Figs. 15 and 16, where $\langle n_e \rangle$ versus $\bar{n}_e$ is plotted for the density profiles obtained in Pulsator and ASDEX, respectively.

The ion temperature profiles in the two machines are different in character. In Pulsator, the T_i profiles are nearly parabolic at low density and become progressively similar to the T_e profiles with increasing n_e. In ASDEX, we find $T_i \sim T_e$ within the entire density regime. In all cases, however, the profiles of the ion temperature are less peaked than those of the electron temperature and T_i exceeds T_e near the boundary. In the case of Pulsator, the radius $r_=$ at which $T_i = T_e$ amounts to typically 8 cm at low, and typically 5 cm at high density, whereas it does not vary markedly in the case of ASDEX.

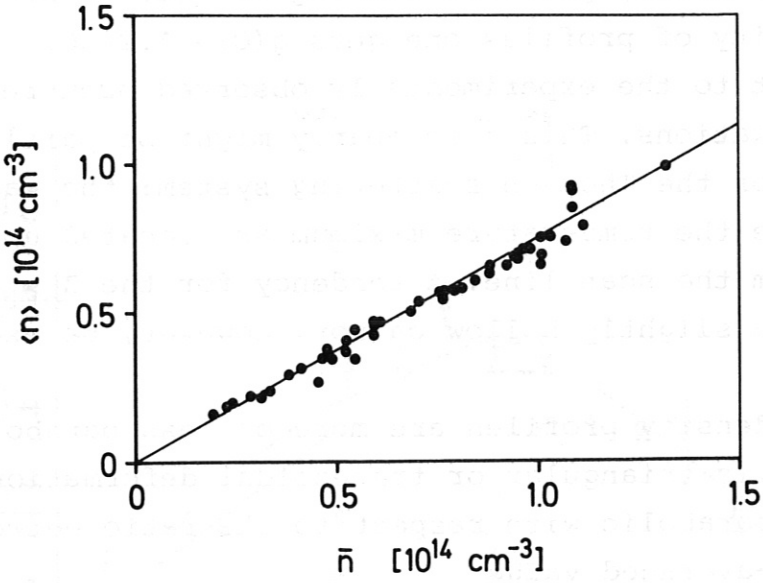

Fig.15: Pulsator.
Cross-section-averaged density <n> versus line-averaged density $\bar{n}$. The slope of the line is 3/4, which holds for parabolic profiles.

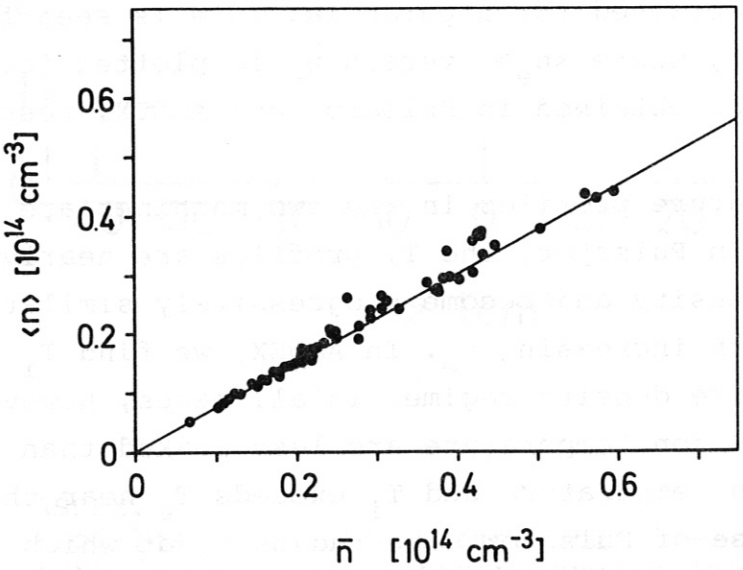

Fig.16: ASDEX.
Cross-section-averaged density <n> versus line-averaged density $\bar{n}$. The slope of the line is 3/4, which holds for parabolic profiles.

As a consequence, the local power transfer p_{ei} from the electrons to the ions changes the sign at $r_=$ so that

$$P_{ei}(r) = \int_0^r p_{ei}(r')\, \pi\, dr'^2$$

is maximal at that radius. In most cases, except at the lowest densities in Pulsator, the values of P_{ei} calculated from the T_e and T_i profiles even become negative at large radii, which is due to systematic errors in the T_i measurement /1o/. In any case, P_{ei}(3a/4) is practically zero as compared with EJ. This means that the fraction of the ohmic heating power which is transferred to the ions in the central regions is conducted to the outer zones, where it is redeposited prior to being transported by ion heat conduction across the plasma boundary.

This has appreciable consequences for the study of the confinement behaviour:

- The ion energy confinement time $\tau_{Ei}(r)$ defined by eq. (3b) becomes meaningless.
- The role of the ion losses is reflected in the radial dependence of the electron energy confinement time $\tau_{Ee}(r)$, which is defined by eq. (2b).
- $\tau_{Ee}(r)$ can be determined fairly well at large radii, but the values become progressively ambiguous for $r < a/2$.
- The energy confinement time $\tau_E \equiv \tau_E(a)$ exceeds $\tau_{Ee} \equiv \tau_{Ee}(a)$ by a factor $1 + \gamma_E$, where

$$\gamma_E = \frac{\int_0^a n_i kT_i\, \pi\, dr^2}{\int_0^a n_e kT_e\, \pi\, dr^2} \quad .$$

The density of the protons is supposed to be proportional to that of the electrons. The proportionality factor is derived by assuming only one species of impurity ions, namely fully stripped oxygen. The relation

$$n_i = \frac{8 - Z_{eff}}{7} n_e \tag{11}$$

is thus used to approximate the proton density.

With this assumption, the profile of the plasma pressure

$$p(r) = n_e(r) \left[kT_e(r) + \frac{8 - Z_{eff}}{7} kT_i(r) \right] \tag{12}$$

can be calculated. Obviously, a broadening of the T_e profiles results both in broader pressure and broader current density profiles. It is most surprising, nevertheless, that the profiles of the pressure and current density are proportional to each other with an accuracy of 5 %. This holds for discharges with $T_i \ll T_e$ as well as for discharges with $T_i \sim T_e$. Thus, the profile functions

$$\hat{n}_e = \frac{n_e(r)}{n_e(o)} \quad , \quad \hat{T}_e = \frac{T_e(r)}{T_e(o)} \quad , \quad \hat{T}_i = \frac{T_i(r)}{T_i(o)}$$

are interlinked by the relation

$$\hat{n}_e = \frac{\hat{T}_e^{3/2}}{\hat{T}_e + \hat{T}_i \frac{n_i(o)\ T_i(o)}{n_e(o)\ T_e(o)}} \quad . \tag{13}$$

A similar relation between the density and the temperature profiles is predicted by the classical theory, if the momentum transfer between electrons and ions due to the electron temperature gradient is taken into account /12/. The Nernst effect, i.e. the component of the friction force which is normal to $\underline{B}$ and ∇T_e, leads for a cylindrical plasma to

$$v_r = -\frac{1}{\sigma_\perp B^2}\left(\frac{\partial p}{\partial r} - \frac{3}{2} n_e \frac{\partial k T_e}{\partial r}\right) \tag{14}$$

allowing for stationary density distributions with $v_r = 0$, i.e. without particle sources within the plasma.

In the case $v_r = 0$, eq. (14) constitutes a relation between the density and the temperature profiles. Plasmas of this kind were realized in cylindrical arcs with superimposed magnetic fields /13,14/. For a hydrogen plasma with $n_i = n_e$ this relation reads $n_e \propto T_e^{1/2}$ if $T_i \ll T_e$ in agreement with eq. (13). For $T_i = T_e$, however, we find $n_e \propto T_e^{-1/4}$ in clear contradiction to the experimental findings.

It is beyond the scope of this paper to speculate whether or not a non-classical modification of the Nernst effect might account for the relation given by eq. (13). In any case, the radial velocity becomes remarkably small at high density.
In the Pulsator device, the particle confinement time

$$\tau_p(r) = \frac{\int_0^r n_e(r')\, 2\pi r' dr'}{\int_0^r n_e(r')\, n_0(r')\, S_i(r')\, 2\pi r' dr'} \tag{15}$$

was studied, Here $S_i(r)$ is the rate coefficient for ionization and $n_o(r)$ the neutral particle density which was deduced from the charge exchange flux spectra /9/. In the density range $1.8 \times 1o^{13} cm^{-3} \leq n_e(0) \leq 1.8 \times 1o^{14} cm^{-3}$ the total particle confinement time only varies from 8 to 11 ms, whereas the central value $\tau_p(0)$ increases from 3o to 1ooo ms, which is obviously due to the rapid decrease of the central neutral density, namely from $1o^9$ to $3 \times 1o^7 cm^{-3}$. The measurement of a particle confinement time as large as 1 s, i.e. 2o times the pulse duration, might be subject to substantial errors. The same holds for ASDEX, where $n_o(0)$ attains even smaller values, namely $1 \times 1o^7 cm^{-3}$ /1o/. Nevertheless, these values indicate the smallness of the particle source term in the central region.

Thus, it remains to be explained why the shape of the density profiles does not vary while that of the source term changes drastically with increasing density. In the context of this paper, we may draw two conclusions: The excess of the particle confinement time in the central region above the energy confinement time means that the energy losses due to the particle flow are much smaller than those due to heat conduction and can therefore be neglected. The second conclusion refers to the energy confinement time $\tau_E(r)$ defined by eq. (7). As a consequence of eq. (13), $\tau_E(r)$ is constant over the minor radius. Furthermore, the current density and the pressure are characterized by the same profile parameter. If we define

$$\langle f \rangle = \frac{1}{\pi a^2} \int_0^a f(r)\, 2\pi r\, dr \tag{16}$$

we find that the profile parameter

$$q' \equiv \frac{q(a)}{q(o)} = \frac{j(o)}{\langle j \rangle} \tag{17}$$

describes the broadness of the pressure profile:

$$q' \equiv \frac{q(a)}{q(o)} = \frac{p(o)}{\langle p \rangle} \quad . \tag{18}$$

In the following, eq. (18) will be used to establish the connection between the central and the averaged pressure.

In many cases, the T_e profile can be approximated by the simple class of functions

$$\hat{T}_e(\rho) = (1-\rho^2)^{\Theta_e} \quad ; \quad \rho = \frac{r}{a} \quad . \tag{19}$$

At uniform E and Z_{eff}, the toroidal current density is then

$$j_\varphi(\rho) = \frac{2 B_\varphi}{\mu_0 R \cdot q(o)} (1-\rho^2)^{3\Theta_e/2} \quad . \tag{2o}$$

Thus

$$q' = \frac{3}{2}\Theta_e + 1 \quad . \tag{21}$$

Generally, more complicated functions are needed to fit the experimental data sufficiently well; the simple functions given by eqs. (19) and (2o), however, are very useful for discussing the integral behaviour of the profiles. It can be shown, for example, that lack of knowledge of the T_e profiles at $\rho > 3/4$ does not impair the accuracy of the energy

balance. In the case $q' = 4$ (corresponding to $\Theta_e = 2$) 96 % of the plasma current flows inside the surface $\rho = 3/4$; hence 96 % of the ohmic power deposition occurs at $\rho = 3/4$. Likewise, 96 % of the plasma energy resides inside this surface. The q value at $\rho = 3/4$ is 2.35.

From eq. (13) it follows that the density profile is correlated to the electron and ion temperature profiles. Using the simple profile functions (19) and

$$\hat{n}_e(\rho) = (1-\rho^2)^\nu \tag{22}$$

we find in both limiting cases $T_i \ll T_e$ and $T_i \sim T_e$ that $\nu = \Theta_e/2$. This does not contradict the near-parabolic character of the density profiles stated above: If $q' = 4$, eq. (13) yields $\Theta_e = 2$, $\nu = 1$. In Pulsator, the value of q_a varies between 2.7 and 5.4. It will be shown in Section 5 that q' can be approximated by $q_a + 1$. Hence $1.8 \leq \Theta_e \leq 3.6$. From

$$\langle n_e \rangle = \frac{1}{\nu+1}\, n_e(0)$$

and

$$\bar{n}_e = \frac{\sqrt{\pi}}{2}\, \frac{\Gamma(\nu+1)}{\Gamma(\nu+3/2)}\, n_e(0) \tag{23}$$

we find that within the q_a range cited above the ratio $\langle n_e \rangle / \bar{n}_e$ only varies between 0.79 and 0.60.

In the cases in which only the central ion temperature $T_i(0)$ was measured, the T_i profiles are approximated by the following procedure: Starting at $\rho = 0$, T_i is assumed to be proportional to n_e out to the radius $\rho_=$ at which this assumption leads to $T_i = T_e$; at $\rho > \rho_=$, it is assumed that $T_i = T_e$. The "profile points" obtained in this way are then subjected to the same fit procedure as is applied to the measured $T_i(\rho)$ points. The artificial T_i profiles obtained in this way satisfy eq. (13) with the same accuracy as the real T_i profiles do. Hence, this procedure is justified as far as the integral behaviour is concerned.

4. PARAMETER DEPENDENCE OF THE ENERGY CONFINEMENT TIME AND OF THE SUM OF THE TEMPERATURES

The values of the energy confinement time $\tau_E \equiv \tau_E(a)$ obtained in the Pulsator and ASDEX devices are plotted versus the line-averaged density $\bar{n}_e$ in Figs. 17 and 18, respectively. As is seen from Figs. 15 and 16, a plot versus $\langle n_e \rangle$ would correspond to a transformation of the abscissa only. In order to distinguish between the discharge types different symbols are used. For the Pulsator data of Fig. 17, S-type profiles are denoted by circles, A-type profiles by triangles. If shaded symbols are used, the ion temperature profile is measured; τ_E values derived from $T_i(0)$ and the extrapolation procedure described in Section 3 are denoted by blank symbols. In the case of the ASDEX data, blank symbols are also used for the τ_E values obtained by assuming $T_i(0) \sim T_e(0)$. In Fig. 18, D-type discharges are denoted by circles, DP-type ones by squares, and discharges with a material limiter (L and LD) by triangles. The data sets are listed in Tables 2 and 3 in the Appendix.

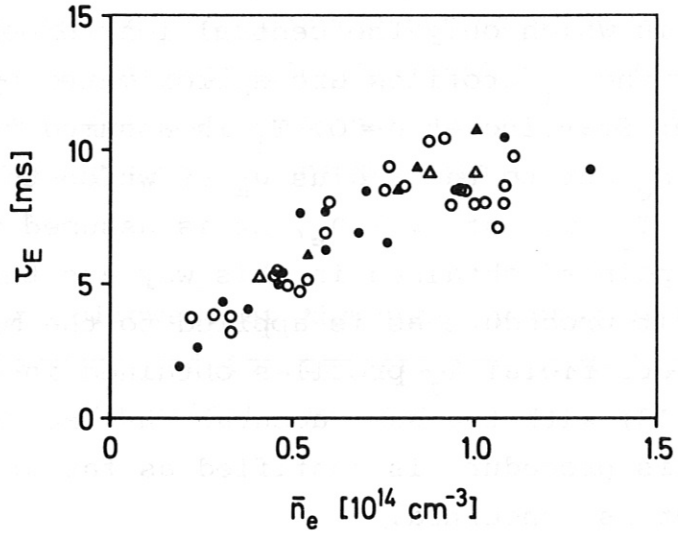

Fig.17: Pulsator.
Energy confinement time τ_E versus $\bar{n}_e$.
O: S-type profiles, Δ: A-type profiles.
Data points based on ion temperature profiles are denoted by shaded symbols; if only the central ion temperature is measured blank symbols are used.

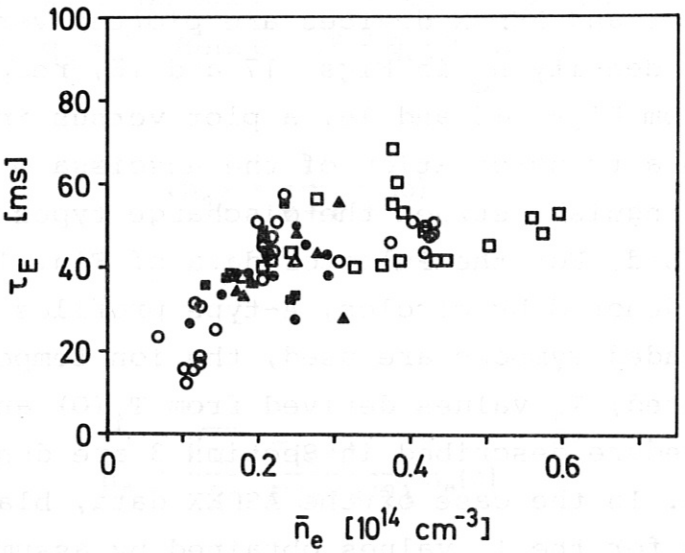

Fig.18: ASDEX.
Energy confinement time τ_E versus $\bar{n}_e$.
O: D-type discharges. □: DP-type discharges.
Δ: Limiter discharges. Data points based on ion temperature profiles are denoted by shaded symbols; if only the central ion temperature is measured blank symbols are used.

It is seen from both Fig. 17 and 18 that τ_E increases linearly with $\bar{n}_e$ at low densities, but tends to saturate. In the case of ASDEX the saturation is apparent; in the case of Pulsator the τ_E versus $\bar{n}_e$ curve begins to saturate at the upper end of the accessible density regime. Furthermore, it is seen from both figures that the scatter of the data cannot be attributed to different confinement properties of different discharge types.

In the following we shall discuss the parameter dependence of the electron energy confinement time, which, according to eq. (2b), is

$$\tau_{Ee} \equiv \tau_{Ee}(a) = \frac{\frac{3}{2}\int_0^a n_e k T_e \pi \, dr^2}{E \cdot I - P_{ei}(a)} \quad . \tag{24}$$

It was shown in the preceding section that $P_{ei}(a) \ll EJ$ at all densities for both devices. In Figs. 19 and 2o, τ_{Ee} is plotted versus $\bar{n}_e$ for Pulsator and ASDEX, respectively, with $P_{ei}(a) = 0$. The discussion of these two curves is the main aim of this section. This is done according to the following guideline: The results presented in Section 3 show that energy losses due to convection can be neglected. Heat conduction is thus the dominant loss mechanism so that the steady-state energy balance equation can be reduced to

$$-\frac{1}{r}\frac{\partial}{\partial r}\left(r\, n_e \chi_e \frac{\partial k T_e}{\partial r}\right) = j(r) \cdot E - p_{ei}(r) \quad . \tag{2c}$$

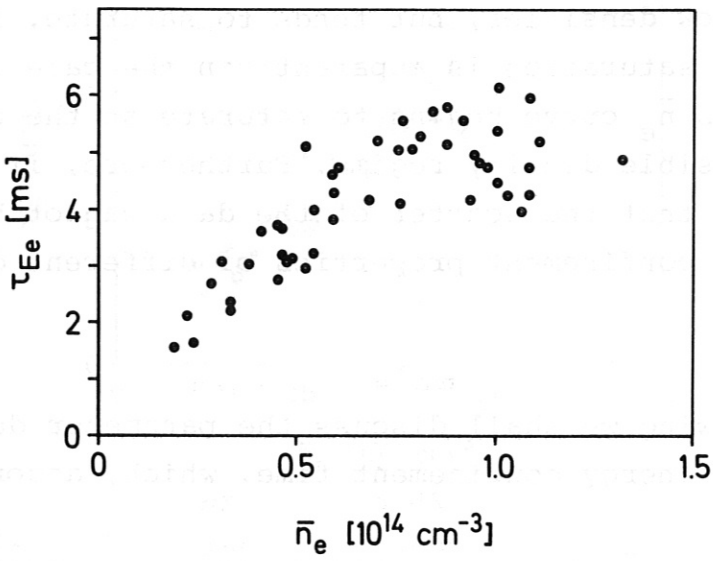

Fig.19: Pulsator.
Energy confinement time of the electrons versus $\bar{n}_e$.

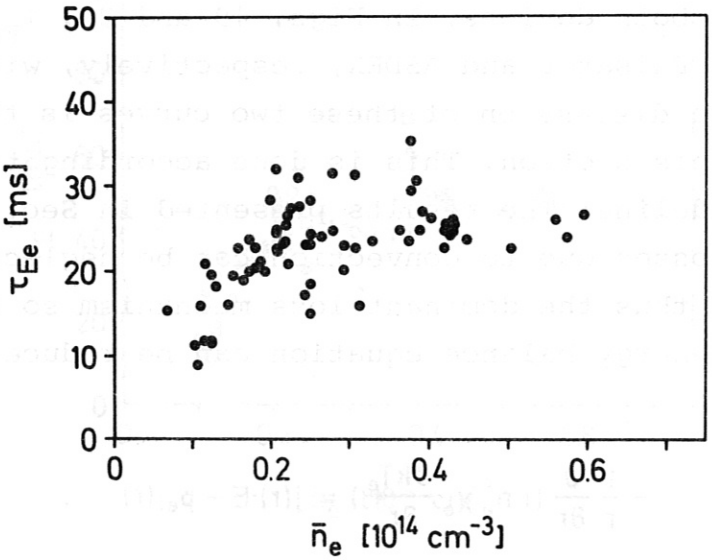

Fig.2o: ASDEX.
Energy confinement time of the electrons versus $\bar{n}_e$.

Let us now suppose that $p_{ei}(r) \ll j(r)E$ is satisfied at all radii, and that the heat conductivity

$$\varkappa_e = n_e \chi_e$$

does not depend on the density. Under these conditions, the electron temperature does not depend on the density either. In the following, we shall investigate whether such a regime can be identified. For this purpose, we consider separately the parameter dependence of the constituents of τ_{Ee}, namely EJ and

$$\frac{3}{2}\int_0^a n_e k T_e \pi \, dr^2 \equiv \frac{3}{2}\langle p_e \rangle \pi a^2 \quad .$$

In Figs. 21, 22 and 23, 24 $3\langle p_e \rangle \pi a^2/2$ and EJ are plotted versus $\bar{n}_e$ for Pulsator and ASDEX, respectively. It is seen that for both Pulsator and ASDEX the decrease of the electron temperature caused by the increase of the density is reflected in the increase of the ohmic heating power EJ.

For the sake of comparison, the total energy content per unit length

$$\frac{3}{2}\langle p \rangle \pi a^2 = \frac{3}{2}\langle p_e + p_i \rangle \pi a^2$$

is also plotted in Figs. 25 and 26. In Pulsator, the ion temperature rises with density so that $\langle p \rangle$ is proportional to $\bar{n}_e$ in good approximation. In other words, the sum

$$T_S = T_e + T_i$$

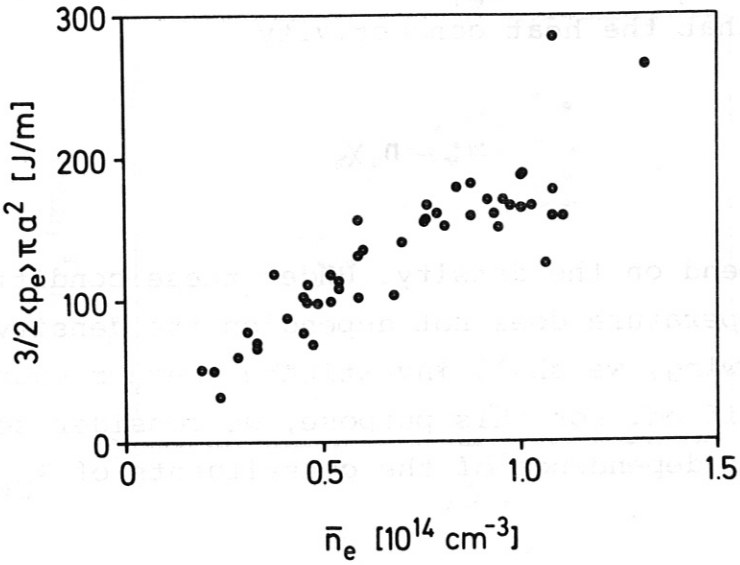

Fig.21: Pulsator.
Electron energy content per unit length versus $\bar{n}_e$.

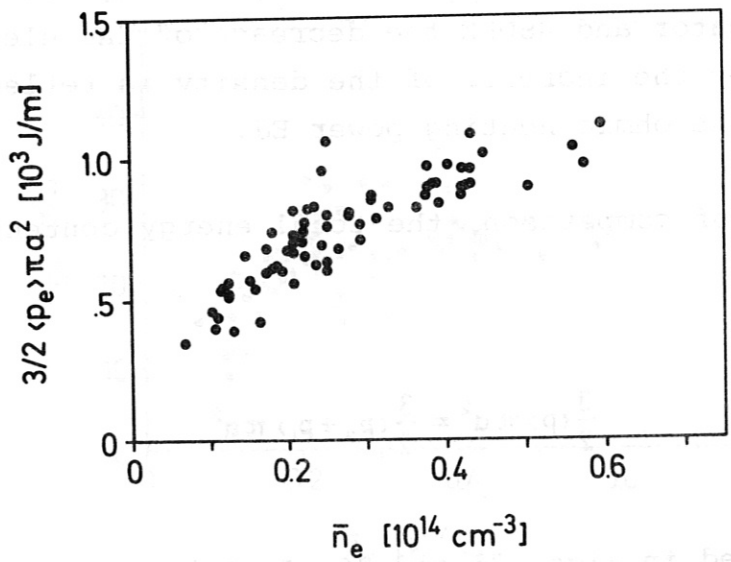

Fig.22: ASDEX.
Electron energy content per unit length versus $\bar{n}_e$.

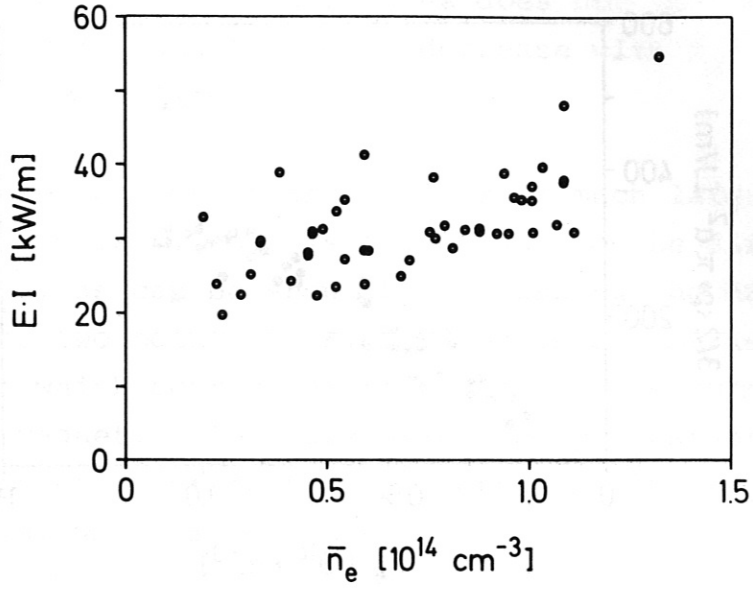

Fig.23: Pulsator.
Heating power EI per unit length versus $\bar{n}_e$.

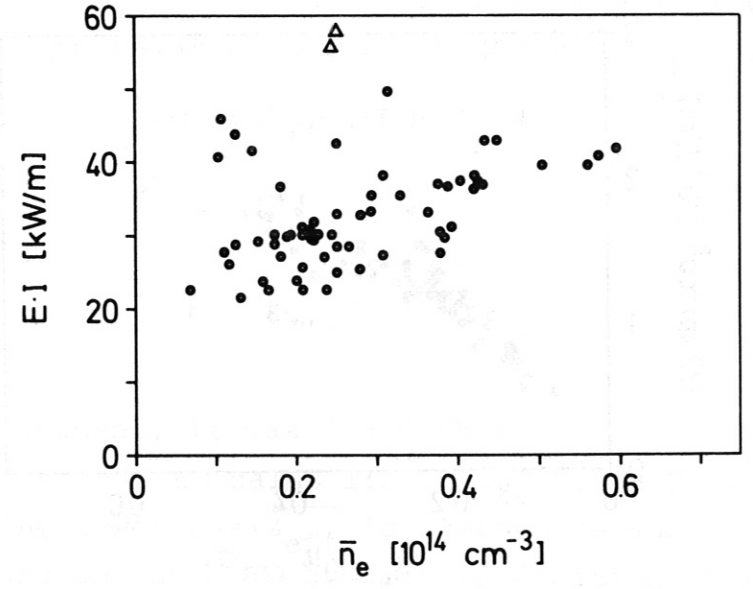

Fig.24: ASDEX.
Heating power EI per unit length versus $\bar{n}_e$.
O: $q_a \sim 4 \div 4.6$, Δ: $q_a = 2.2$.

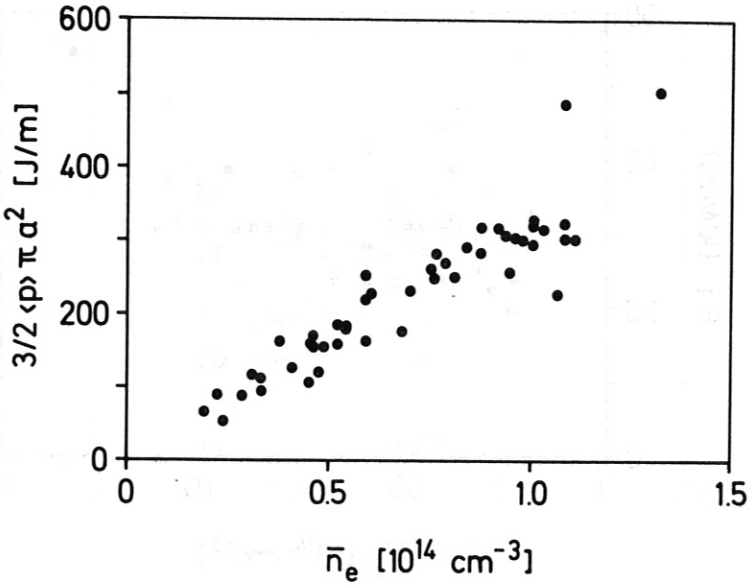

Fig.25: Pulsator.
Energy content per unit length versus $\bar{n}_e$.

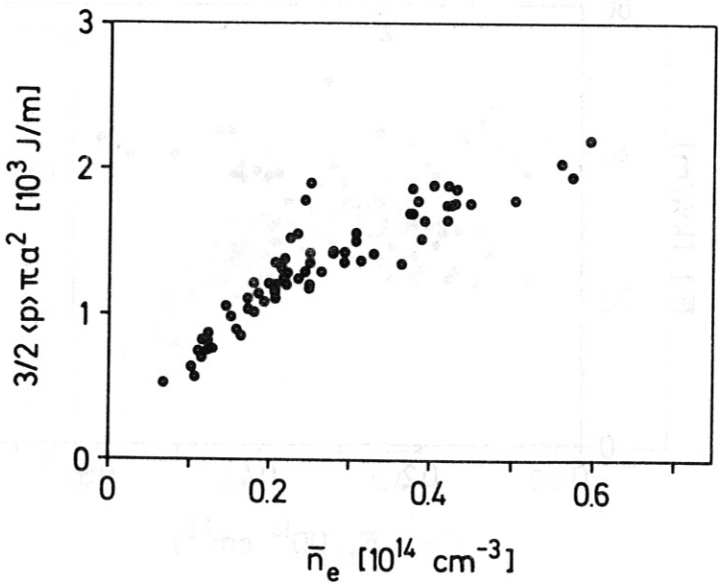

Fig.26: ASDEX.
Energy content per unit length versus $\bar{n}_e$.

of the electron and ion temperatures does not vary with the density. In ASDEX, both T_e and T_i decrease with n_e; hence <p> rises less than linearly.

Apparently, the scatter of the EJ data is much larger than that of the energy content. This is mainly due to the different values of Z_{eff}, as can be shown by discussing the ASDEX plots: Apart from the two points in Fig. 23 which are marked by triangles and which correspond to J = 4oo kA the current and the toroidal magnetic field are practically constant (24o - 26o kA; 22 kG). The power input is thus proportional to the toroidal electric field, which is given by

$$E = \frac{j(o)}{\sigma(o)} = \frac{2 B_\varphi}{\mu_o R q(o)} \cdot \frac{Z_{eff}}{\sigma^* k T_e^{3/2}(o)} \qquad (25)$$

where σ^* is a constant. An enhancement of Z_{eff} leads to larger temperatures; hence E does not grow proportionally to Z_{eff}. Describing the correlation between $T_e(0)$ and Z_{eff} by

$$T_e(o) = Z_{eff}^{\alpha} \cdot f(I, B_\varphi, \ldots.)$$

we get

$$E = (Z_{eff} \cdot f)^{1-3\alpha/2}$$

Varying the exponent, it was found that $\alpha = 1/3$ fits the ASDEX data best; thus E scales like $Z_{eff}^{1/2}$. In Fig. 27, the reduced heating power $EJ/\sqrt{Z_{eff}}$ is plotted versus $\bar{n}_e$ for ASDEX. It is seen that the scatter of data is drastically reduced; only the 4oo kA points (triangles) are left above the bulk. The smoothing effect on the central electron temperature is

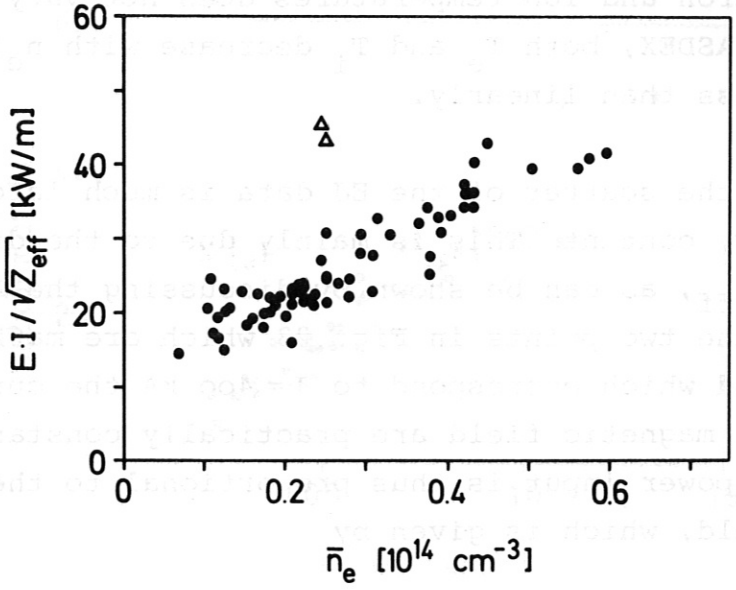

Fig.27: ASDEX.
Reduced heating power $EI/\sqrt{Z_{eff}}$ per unit length versus $\bar{n}_e$. O: $q_a \sim 4 \div 4.6$; Δ: $q_a = 2.2$.

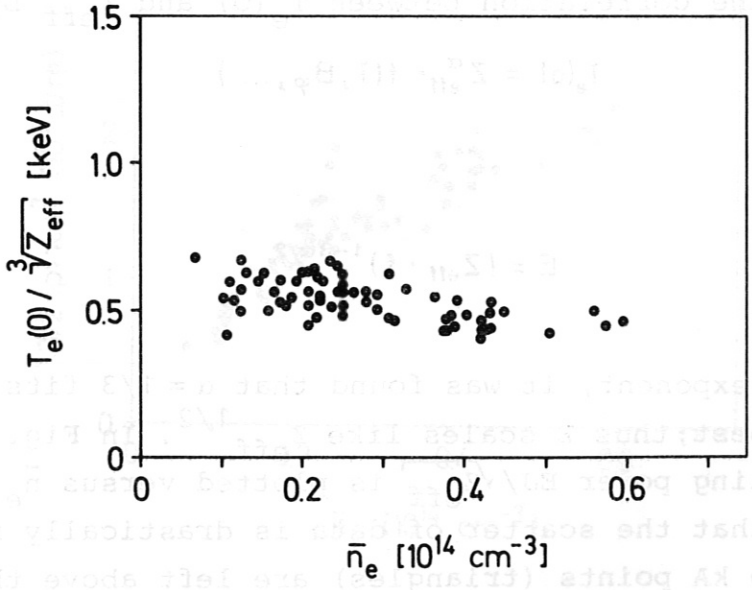

Fig.28: ASDEX.
Reduced central electron temperature $T_e(0)/\sqrt[3]{Z_{eff}}$ versus $\bar{n}_e$.

shown in Fig. 28, where $kT_e(0)/\sqrt[3]{Z_{eff}}$ is plotted versus $\bar{n}_e$, again for ASDEX. This figure ought to be compared with Fig.6, in particular with the points denoted by triangles which are obtained from discharges with $Z_{eff} \leq 1.3$. Apparently, $T_e(0) = Z_{eff}^{1/3} f(I, B_\varphi, ..)$ describes the Z_{eff} dependence of the electron temperature fairly well. Since the ions are closely coupled to the electrons, the same relation must also hold for the ion temperature. In the following, we shall apply this "scaling law" to the Pulsator data, too.

As for the energy content, we replace $\langle p_e \rangle$ and $\langle p \rangle$ by the "average over the particles" of T_e and $T_s = T_e + T_i$, namely

$$\{kT_e\} = \frac{\langle nkT_e \rangle}{\langle n \rangle} \quad , \quad \{kT_s\} = \frac{\langle nk(T_e+T_i) \rangle}{\langle n \rangle} \quad .$$

We thus try to achieve linear plots of the quantities

$$EI\ Z_{eff}^{-1/2}\ q_5^{\gamma_1}\ B_{25}^{\beta_1}$$

$$\{kT_e\} Z_{eff}^{-1/3}\ q_5^{\gamma_2}\ B_{25}^{\beta_2} \quad , \quad \{kT_s\} Z_{eff}^{-1/3}\ q_5^{\gamma_2}\ B_{25}^{\beta_2} \quad .$$

versus $\bar{n}_e$ where we introduced

$$q_5 \equiv \frac{q'}{5} = \frac{q_a + 1}{5} \quad , \quad B_{25} \equiv \frac{B_\varphi}{25\ kG} \quad .$$

In the search for the best fit one has to bear in mind that q_5 only varies by a factor of 2, and B_{25} even less, namely by a factor of 1.3. The exponents β_1, β_2, γ_1, γ_2 thus cannot be determined with high accuracy; the error is estimated to be ± 0.25. Hence the exponents were only varied in steps of 0.25. The best fit was found by choosing $\beta_1 = -1/2$, $\beta_2 = -1$, $\gamma_1 = 1$, $\gamma_2 = 3/4$.

The reduced ohmic heating power per unit length, namely

$$(E\cdot I)^* = \frac{E\cdot I\cdot q_5}{B_{25}^{1/2}\, Z_{eff}^{1/2}} \qquad (26)$$

is plotted versus $\bar{n}_e$ in Figs. 29 and 3o for Pulsator and ASDEX, respectively. In the case of Pulsator, it is seen that $(EJ)^*$ is practically constant up to $\bar{n}_e = 0.8 \times 1o^{14} cm^{-3}$ and grows proportionally to $\bar{n}_e$ at higher density; the lines plotted in Fig. 29 are given by

$$(E\cdot I)^* = \begin{cases} 20\,\frac{kW}{m} & ;\ \bar{n}_{14} \leq 0.8 \\ 25\,\bar{n}_{14}\,\frac{kW}{m} & ;\ \bar{n}_{14} \geq 0.8 \end{cases}$$

where

$$\bar{n}_{14} = \bar{n}_e / 10^{14}\, cm^{-3} \ .$$

In the case of ASDEX, $(EJ)^*$ grows monotonically with density and can be described fairly well by the line

$$(E\cdot I)^* = (1 + 4.85\,\bar{n}_{14})\cdot 12\,\frac{kW}{m} \ .$$

The reduced, particle-averaged electron temperature

$$\{kT_e\}^* = \frac{q_5^{3/4}\ \{kT_e\}}{B_{25}\ Z_{eff}^{1/3}} \qquad (27)$$

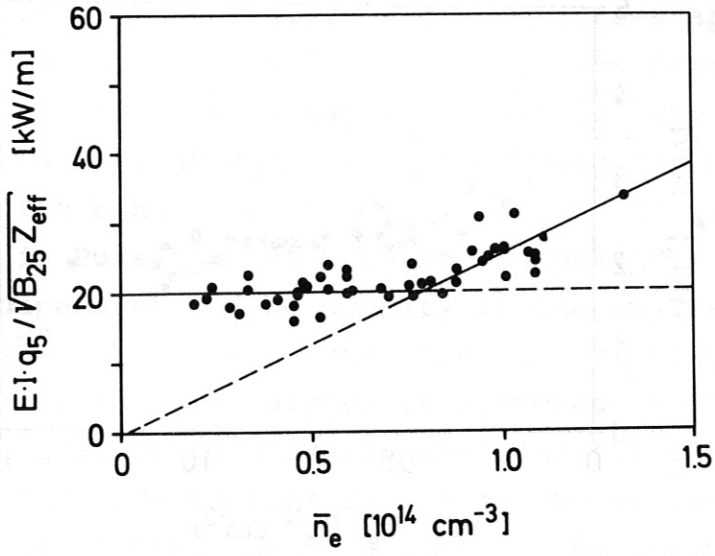

Fig.29: Pulsator.
Reduced heating power per unit length versus $\bar{n}_e$.

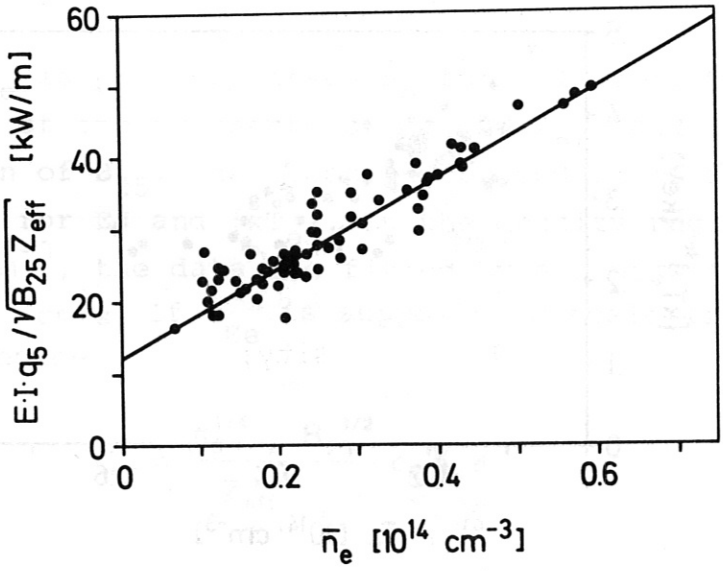

Fig.3o: ASDEX.
Reduced heating power per unit length versus $\bar{n}_e$.

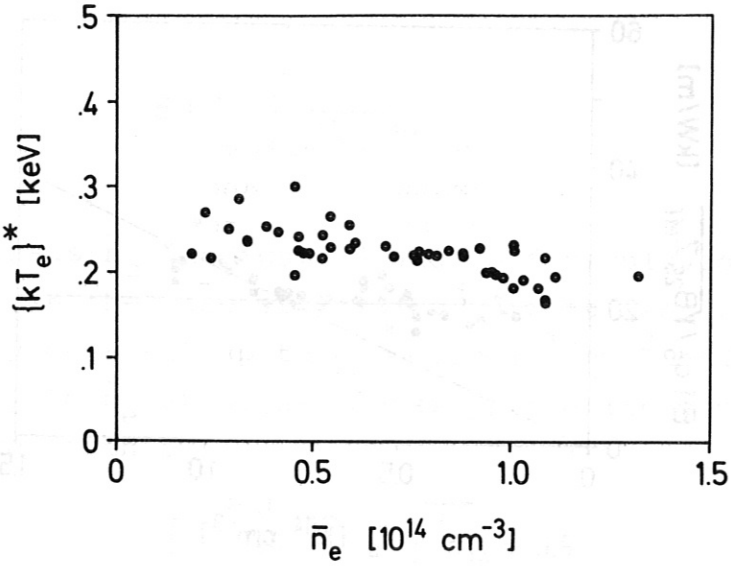

Fig.31: Pulsator.
Particle-averaged electron temperature reduced according to eq. (27).

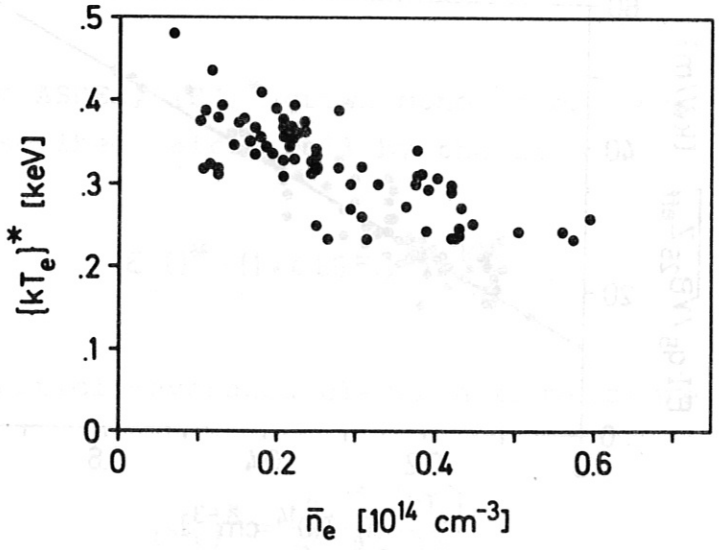

Fig.32: ASDEX.
Particle-averaged electron temperature reduced according to eq. (27).

is plotted versus $\bar{n}_e$ in Figs. 31 and 32 for Pulsator and ASDEX, respectively. Apparently, $\{kT_e\}^*$ decreases appreciably in the case of ASDEX, whereas it is a very weak function of the density in the case of Pulsator; in particular, it is approximately constant at densities below $0.8 \times 10^{14} cm^{-3}$ in agreement with the behaviour of $(EJ)^*$. We thus arrive at the statement that in Pulsator the electron temperature is practically independent of the density in the regime $\bar{n}_e \lesssim 0.8 \times 10^{14} cm^{-3}$, which means that the energy balance at these densities is only marginally affected by the power transfer to the ions.Hence the data obtained for the electron energy confinement time in this regime can be exclusively attributed to the electron heat conduction. In combining eqs. (26) and (27) it is seen that the reduced electron energy confinement time is given by

$$\tau_{Ee}^* = \frac{Z_{eff}^{1/6}}{B_{25}^{1/2}\, q_5^{1/4}}\, \tau_{Ee} \quad . \tag{28}$$

In Fig. 33, τ^*_{Ee} is plotted versus $\bar{n}_e$ for Pulsator. Owing to the smallness of the exponents of q_5 and Z_{eff} and to the small variation of B_{25}, the smoothing procedure is far less efficient than for EJ and $\{kT_e\}$. In the density regime $\bar{n}_e \lesssim 0.8 \times 10^{14} cm^{-3}$, the data are fitted by a line with the slope $7.7 \times 10^{-17} cm^3 s$. If τ_{Ee} is supposed to scale like a^2 we get for this regime

$$\tau_{Ee} = \frac{q_5^{1/4}\; B_{25}^{1/2}}{Z_{eff}^{1/6}}\, c_p\, \bar{n}_e\, a^2 \tag{29}$$

where $c_p = 0.64 \times 10^{-18} cm\ s$, this value being a factor of 1.6 larger than that of the so-called Alcator scaling /15,16/.

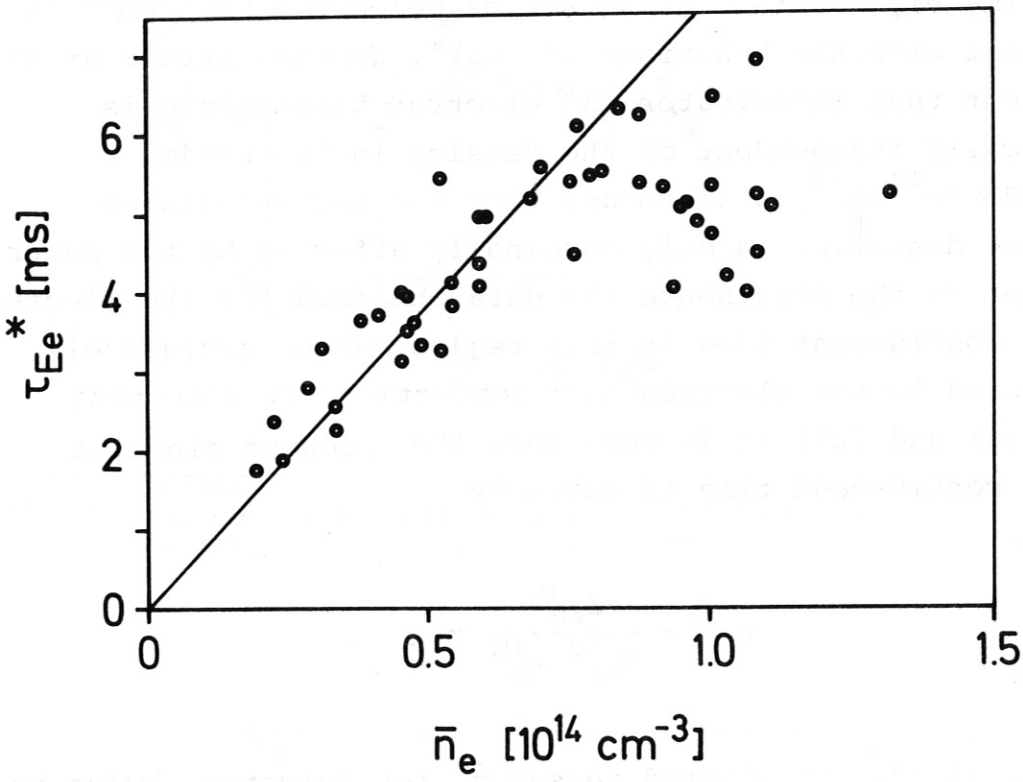

Fig.33: Pulsator.
Reduced electron energy confinement time versus $\bar{n}_e$.

(Note that for the typical values $q_5 = 1$, $B_\varphi = 27$ kG and $Z_{eff} = 2$, the factor $q_a^{1/4}\ B_{25}^{1/2}\ Z_{eff}^{-1/6}$ amounts to 0.93.)

As for the ASDEX data, it is seen from both Fig. 3o and 32 that the electron temperature decreases with n_e in the entire density regime covered by the experiments. We conclude from this that the power transfer to the ions is important even at the lowest densities in ASDEX. This conclusion is also supported by the different behaviour of the ion temperature and hence of $T_s = T_e + T_i$ in both devices. In Section 6, it will be shown that the $T_s(0)$ versus $\bar{n}_e$ curves can be compared with simple model calculations. For this reason, the scaling relations describing $\{T_s\}$ will be studied in some more detail.

In Figs. 34 and 35, the function

$$\{kT_s\}^* = \frac{\{kT_s\}\ q_5^{3/4}}{B_{25}\ Z_{eff}^{1/3}} \tag{3o}$$

is plotted versus $\bar{n}_e$ for Pulsator and ASDEX, respectively. Apparently, in the case of Pulsator, $\{kT_s\}^*$ is constant in good approximation; hence the data are fitted well by the horizontal line $\{kT_s\}^* = 365$ eV. In the case of ASDEX, $\{kT_s\}^*$ decreases slightly but systematically with $\bar{n}_e$. The centre of gravity of the data points shown in Fig. 35 is located at $\bar{n}_e = 2.7 \times 1o^{13}\,cm^{-3}$, $\{kT_s\}^* = 573$ eV; hence an attempt was made to describe the density dependence by the ansatz

$$\{kT_s\}^* = 573\ eV \left(\frac{\bar{n}_{14}}{0.27}\right)^{-\lambda} . \tag{31}$$

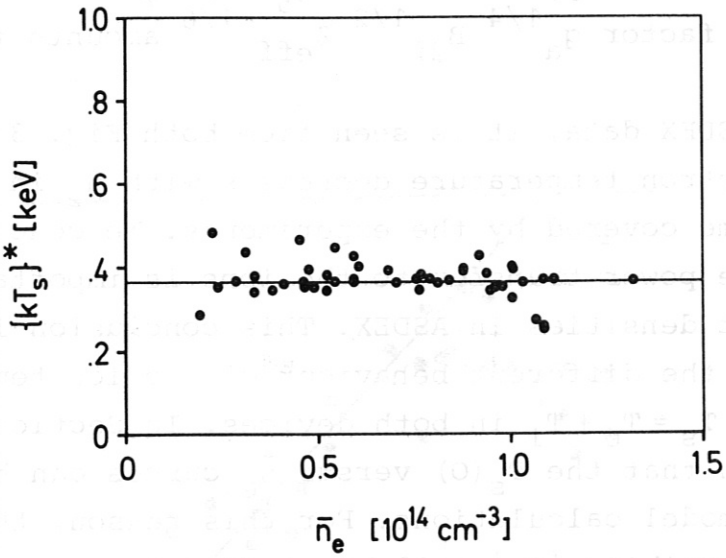

Fig.34: Pulsator.
Particle-averaged sum of electron and ion temperature, reduced according to eq. (3o). The horizontal line denotes $\{kT_s\}^* = 365$ eV.

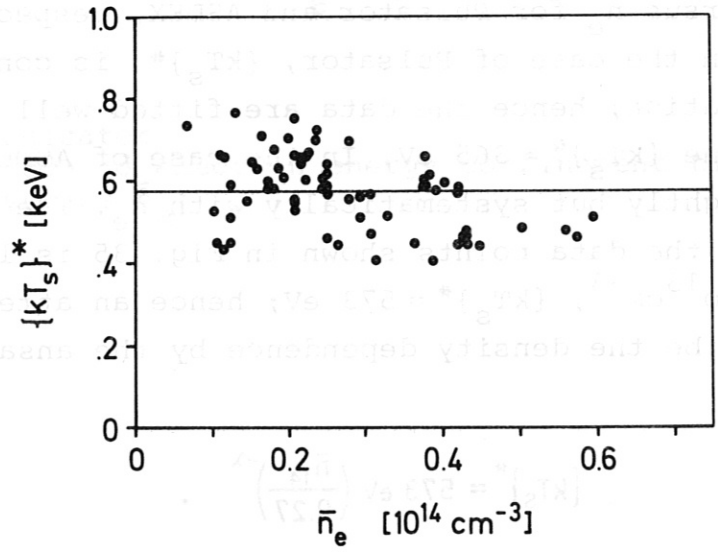

Fig.35: ASDEX.
Particle-averaged sum of electron and ion temperature, reduced according to eq. (3o). The horizontal line denotes $\{kT_s\}^* = 573$ eV.

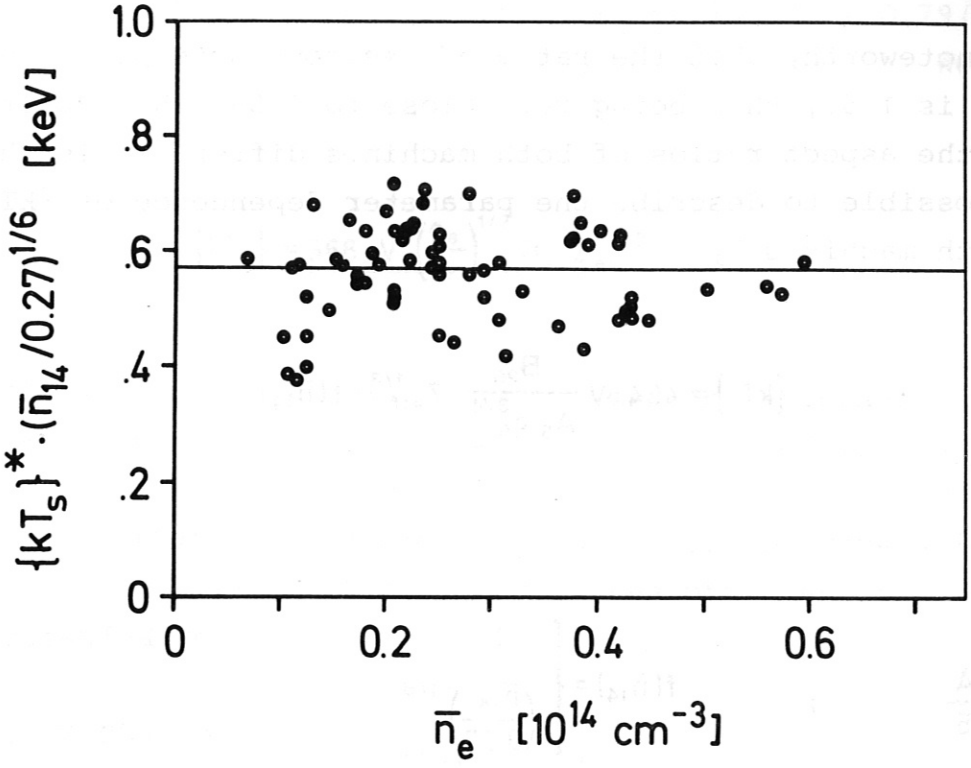

Fig.36: ASDEX.
The data of Fig.35 are multiplied by $(\bar{n}_{14}/0.27)^{1/6}$ and plotted versus $\bar{n}_e$. The horizontal line again denotes $\{kT_s\}^* = 573$ eV.

By tentatively putting $\lambda = 1/4,\ 1/5,\ 1/6,\ 1/10$ the exponent $\lambda = 1/6$ was found to fit the data best; the result is shown in Fig. 36.

It is noteworthy that the ratio of the constants 573 eV and 365 eV is 1.57, this being very close to 1.54, the factor by which the aspect ratios of both machines differ. It is therefore possible to describe the parameter dependence of $\{kT_s\}$ for both machines by

$$\{kT_s\} = 464\ \text{eV}\ \frac{B_{25}}{A_5\, q_5^{3/4}}\, Z_{eff}^{1/3} \cdot f(\bar{n}_{14}) \qquad (32)$$

with

$$A_5 \equiv \frac{A}{5} \quad ; \quad f(\bar{n}_{14}) = \begin{cases} 1 & \text{for Pulsator} \\ \left(\dfrac{\bar{n}_{14}}{0.27}\right)^{-1/6} & \text{for ASDEX} \end{cases} .$$

It was already stated above that B_φ was only varied by a factor of 1.3. Hence the linear dependence of $\{kT_s\}$ on B_φ given by eq. (32) must not be extrapolated to experiments in which B_φ was varied appreciably.

It is seen from eq. (32) that $\{kT_s\}$ is nearly proportional to B_a, the poloidal magnetic field on the plasma boundary. With

$$B_{a1} \equiv B_a / 1\text{kG}$$

we get

$$\{kT_s\} = 464\ \text{eV}\ \frac{q_a}{5\, q_5^{3/4}}\, B_{a1}\, Z_{eff}^{1/3} \cdot f(\bar{n}_{14}) \quad . \qquad (33)$$

In order to simplify the empirical relations, we shall express q_5 by q_a. In the range $2.2 \leq q_a \leq 5.4$, $q_a + 1$ is well approximated by $1.79\ q_a^{3/4}$ and hence $q_a/5q_5^{3/4}$ by $0.43\ q_a^{7/16}$. Furthermore, the latter expression is replaced by $0.79(q_a/4)^{1/2}$ (which is precisely equal to $0.43\ q_a^{7/16}$ for $q_a = 4$). We thus arrive at

$$\{kT_S\} = 366\ \text{eV} \left(\frac{q_a}{4}\right)^{1/2} B_{a1}\, Z_{eff}^{1/3} \cdot f(\bar{n}_{14}) \quad . \tag{34}$$

According to eqs. (32, 33, 34), the particle-averaged sum of the temperatures does not depend on the size of the machines.

For the following discussions it is useful to express $\{kT_s\}$ by $kT_s(0)$, using the relations between the profiles derived in Section 3. It was shown there that

$$\frac{\langle nkT_S \rangle}{n(0)\, kT_S(0)} = \frac{1}{q'}$$

and hence

$$\{kT_S\} = \frac{1}{q'}\, kT_S(0) \cdot \frac{n(0)}{\langle n \rangle} \quad . \tag{35}$$

From the profile functions introduced in Section 3 it follows that

$$\frac{n(0)}{\langle n \rangle} = \nu + 1 = \frac{\Theta_e}{2} + 1 = \frac{q_a + 3}{3} \tag{36}$$

where again $q' = q_a + 1$. For $2.2 \leq q_a \leq 5.4$, the function $(q_a + 3)/3$ is well approximated by $1.18\ q_a^{1/2}$. The combination of eqs. (34), (35) and (36) thus leads to

$$kT_S(o) = 278\ eV\ \ q_a^{3/4}\ B_{a1}\ Z_{eff}^{1/3}\ f(\bar{n}_{14}) \tag{37}$$

or to

$$kT_S(o) = 1388\ eV\ q_a^{-1/4}\ \frac{B_{25}}{A_5}\ Z_{eff}^{1/3}\ f(\bar{n}_{14}) \quad . \tag{38}$$

The parameter dependence of $kT_s(0)$ given by eq. (38) agrees with what one expects: The central temperature increases with the current density, which is proportional to B_φ and with Z_{eff}. Furthermore, broadening of the profiles, indicated by the decrease of q_a, leads to enhancement of the central temperature.

From eq. (38) it follows that the parameter dependence of the central electron temperature must be given by

$$kT_e(o) = const.\ q_a^{-1/4}\ \frac{B_{25}}{A_5}\ Z_{eff}^{1/3}\ g(\bar{n}_{14}) \tag{39}$$

where $g(\bar{n}_{14})$ is again different for Pulsator and ASDEX. On the other hand, $kT_e(0)$ can also be determined from

$$E \cdot I = \frac{4\pi}{\mu_0^2}\ \frac{B_a^2}{\langle\sigma\rangle} = \frac{4\pi\ B_a^2}{\mu_0^2}\ q'\ \frac{Z_{eff}}{\sigma^*\ kT_e^{3/2}(o)} \quad . \tag{4o}$$

Insertion of eq. (26) into this equation leads to

$$kT_e(o) = \text{const.}\ q_a^{2/3} \cdot B_{a1} \cdot Z_{eff}^{1/3} \cdot g(\bar{n}_{14}) \qquad (41)$$

which agrees with eq. (4o) apart from the slightly different dependence on q_a.

Finally, we compare eq. (38) with the experimental data. For the purposes of Section 6 we discuss the density dependence of the mean central temperature namely

$$\frac{1}{2} kT_S(o) = \frac{1}{2} k(T_e(o) + T_i(o)) \quad .$$

According to eq. (38), we introduce

$$\frac{1}{2} kT_S^{**}(o) = s \cdot \frac{q^{1/4}}{B_{25}\ Z_{eff}^{1/3}} \cdot \frac{1}{2}\ kT_S(o) \qquad (42)$$

where the factor s is adjusted so that $T_s^{**}(O) = T_s(O)$ for typical parameters. For Pulsator we choose $B_\varphi = 27$ kG, $q_a = 3$ and $Z_{eff} = 2$; it is seen from Fig.3 that $Z_{eff} = 2$ is practically the average value for all densities. This leads to $s = 1.o34$. In the case of ASDEX we find $Z_{eff} < 1.3$ at densities above $3 \times 1o^{13} cm^{-3}$ (see Figs. 4 and 6); thus we choose $Z_{eff} = 1.15$ and $q_a = 3$, $B_\varphi = 22$ kG resulting in $s = O.7o2$.

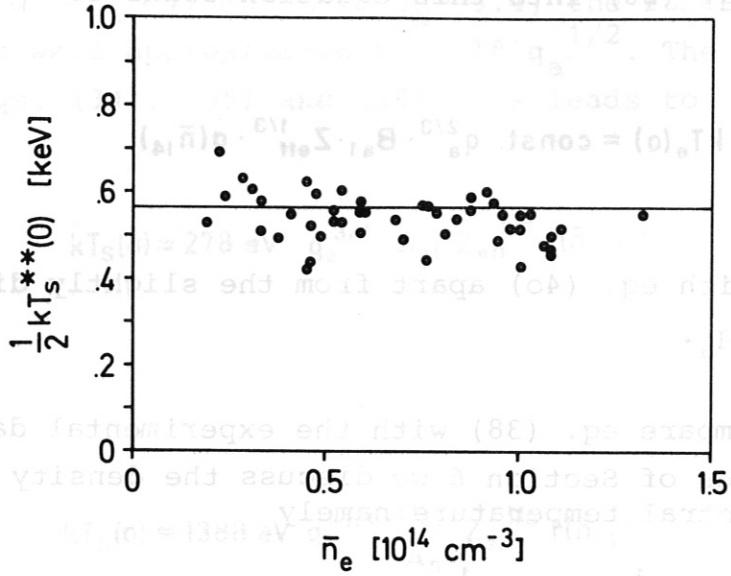

Fig.37: Pulsator.
Half the sum of the central temperatures normalized according to eq. (42).

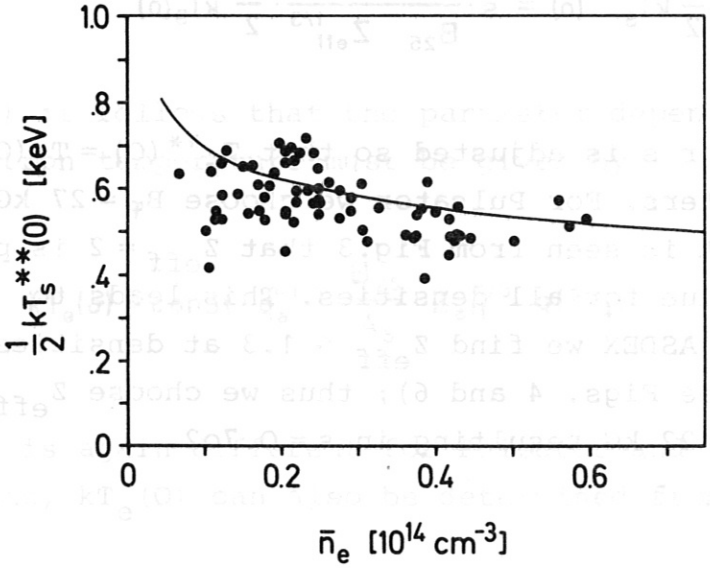

Fig.38: ASDEX.
Half the sum of the central temperatures normalized according to eq. (42).

These data are now compared with 564 eV for Pulsator, and $(0.27/\bar{n}_{14})^{1/6}$. 590 eV for ASDEX. This is done in Figs. 37 and 38. It is seen that in the case of Pulsator the sum of the central temperatures slightly decreases with $\bar{n}_e$, whereas $\{kT_s\}$ stays constant (see Fig. 31). This different behaviour can be attributed to the profile characteristics: The increase of the ion temperature with density affects the particle-averaged value of T_s more than the central one because the T_i profiles are broader than the T_e profiles. It is therefore conceivable that the decrease of $\{T_e\}$ is fully compensated by the increase of $\{T_i\}$, while there is a slight fall of the $T_s(0)$ versus $\bar{n}_e$ curve. In the case of ASDEX, there is no such deviation since T_i is close to T_e at all densities.

Apart from this profile effect, the extrapolation procedure leading from eq. (32) to eq. (38) provides a satisfactory description of $T_s(0)$ as a function of $\bar{n}_e$. In the following section, the influence of the internal disruptions on $T_s(0)$ and on the profiles will be discussed.

5. THE ROLE OF THE SAWTOOTH RELAXATIONS

The majority of the electron density and temperature profiles discussed in Section 3 is subjected to the well-known sawtooth modulation, the exception being the A-type discharges obtained in the Pulsator device. Direct experimental evidence of sawtooth relaxations of the ion temperature is very poor; modulation of the charge-exchange flux was only observed in rare cases. This might be due to the insufficient temporal resolution of this diagnostic. Measurements of the neutron emission rate, which was found to exhibit sawtooth modulations in several tokamaks (see, for example Ref./15/) were performed neither in Pulsator nor in the first year of ASDEX operation.

In this section, the influence of the sawtooth relaxations on the energy confinement is investigated. The most appropriate way is to describe the rising phase of a sawtooth by the non-stationary energy balance equations (2) and (3). Using

$$w_{e(i)}(r) = \frac{3}{2} n(r)\, k\, T_{e(i)}(r)$$

these equations read

$$\frac{\partial w_e}{\partial t} + \frac{w_e}{\tau_{Ee}} = jE - P_{ei} \quad , \tag{2d}$$

$$\frac{\partial w_i}{\partial t} + \frac{w_i}{\tau_{Ei}} = P_{ei} \tag{3d}$$

where again charge exchange and radiation are neglected. Since the temporal variations of the density and temperatures are linear in good approximation, the time derivatives in eqs.(2d) and (3d) can be replaced by $\Delta\overset{\frown}{w}_e/\overset{\frown}{\tau}$ and $\Delta\overset{\frown}{w}_i/\overset{\frown}{\tau}$, where $\Delta\overset{\frown}{w}_e$, $\Delta\overset{\frown}{w}_i$

are the modulations of w_e, w_i and $\tilde{\tau}$ is the sawtooth period. In the following, the density dependence of the data and the way they are taken are dealt with.

The modulation $\Delta\tilde{\bar{n}}_e$ of the line-averaged electron density due to the sawtooth relaxation is clearly seen in the (microwave and infrared) interferometer signals, provided that the number of fringes is not too small. In both devices, $\Delta\tilde{\bar{n}}_e/\bar{n}_e$ amounts to typically 1 % and never exceeds 2 %. Since the sawteeth do not extend to the plasma boundary, the total number of particles is conserved during relaxation. Hence the variation $\Delta\tilde{n}_e(0)/n_e(0)$ of the central electron density can be estimated from $\Delta\tilde{\bar{n}}_e/\bar{n}_e$ using eq. (23). For a parabolic profile ($\nu = 1$) and for variations of the order 10^{-2} the modulation of the central electron density is typically twice the line-averaged one.

The experimental information on the sawtooth modulation of the electron temperature is rather different for both devices; this holds particularly for the diagnostic methods they are obtained from. In the case of ASDEX the Thomson scattering is expected to record profile changes since a profile is obtained by a single laser shot. Unfortunately, the simultaneous measurement at several local points involves the disadvantage of using 10 different detectors for the 10 locations along the laser beam. Systematic deviations of the order of the temperature modulation $\Delta\tilde{T}_e/T_e$ are likely to be present so far. This problem might be overcome by signal averaging over a large series of reproducible discharges.

In contrast to what is expected, the single-point Thomson scattering system of the Pulsator device provided some information on the profile variation. By chance, in a discharge with $q_a = 2.7$ a sufficient number of laser shots occurred in

phase with the sawtooth, i.e. immediately after relaxation. The T_e profile obtained in this way is shown in Fig.39a. For the sake of comparison, Fig.39b presents a T_e profile from the same discharge (taken 2o ms later on) the points of which are distributed at random over the phases of the sawtooth.

In order to follow the temporal evolution of the electron temperature during a sawtooth period, a particular technique based on the reproducibility of the relaxation time was applied. The triggering procedure of the laser was altered in the following manner: Trigger 1 opens a gate at a preset time; if the gate is open, trigger 2 becomes operational. The second trigger is derived from the fast decrease of the X-ray diode signal and is delayed so as to sample selected phases of the sawtooth. A result of this procedure is presented in Figs.4o a and 4o b showing T_e profiles consisting of points obtained in the first and last quarters of a sawtooth, respectively. It is clearly seen from both Figs. 39 and 4o that a flat T_e profile in the central region is characteristic of the situation immediately after the sawtooth relaxation; in the rising phase of the sawtooth, however, the T_e profiles become peaked again.

The temporal variation of the electron temperature was investigated in the Pulsator device, using the standard soft X-ray diode technique. The modulation of the diode signal from the central channel can be ascribed to the parameters at r=0 and can be written in the form

$$\frac{\Delta\tilde{S}}{S} = c_1 \frac{\Delta\tilde{T}_e}{T_e} + c_2 \frac{\Delta\tilde{n}_e}{n_e} \quad . \tag{43}$$

The density modulation $\Delta\tilde{n}_e/\bar{n}_e$ is known from interferometry; hence $\Delta\tilde{T}_e/T_e$ can be deduced from $\Delta\tilde{S}/S$ and is found to amount

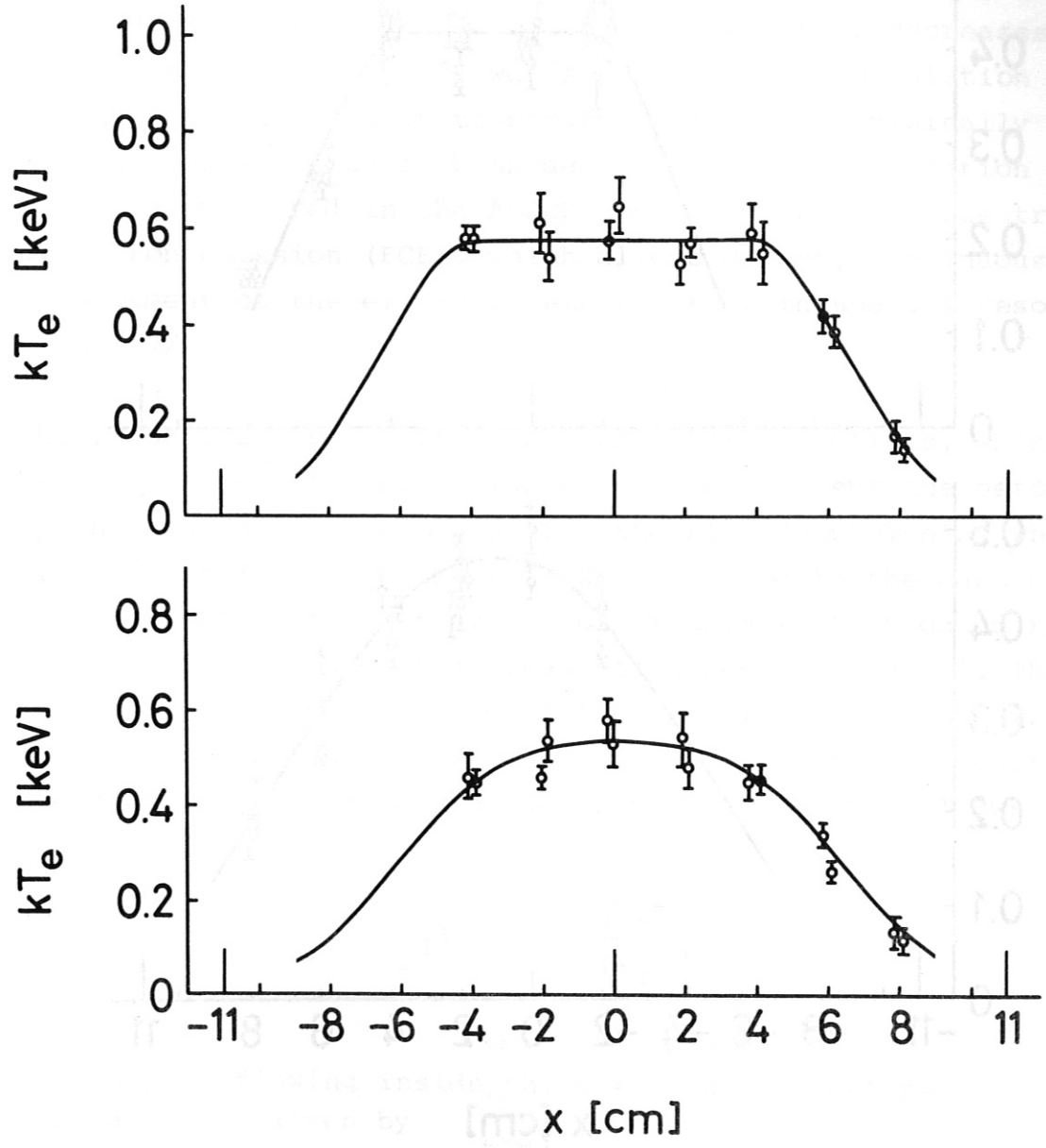

Fig.39: Pulsator.
Above 39a: A T_e profile made up by points taken after a sawtooth relaxation.
Below 39b: A T_e profile made up by points distributed over different phases of the sawtooth.

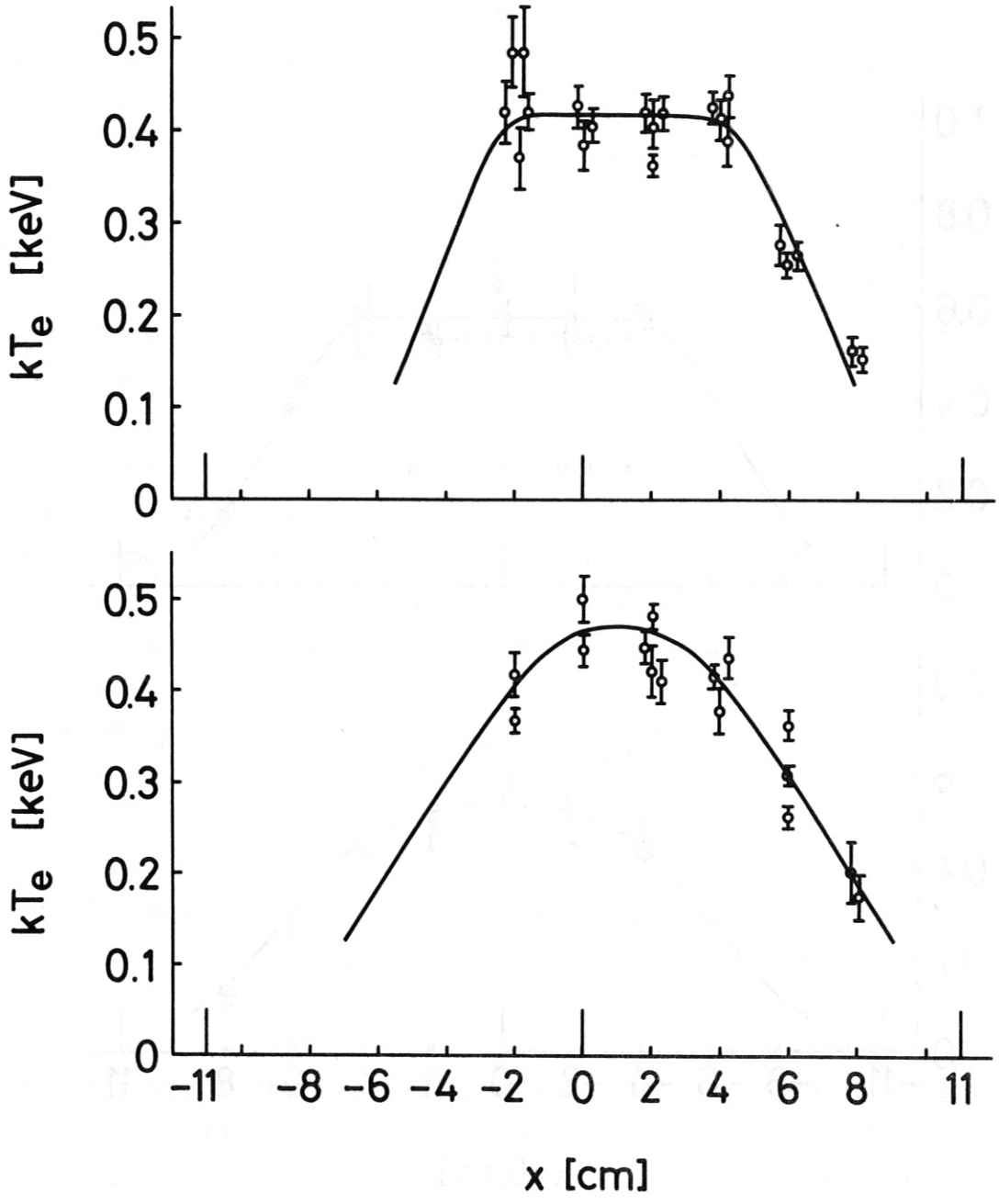

Fig.4o: Pulsator.
Above 4oa: A T_e profile made up by points selected from the first quarter of a sawtooth period.
Below 4ob: A T_e profile made up by points selected from the last quarter of a sawtooth period.

to 1o - 12 % for the central temperature independently of the density. Since the central electron temperature decreases with $\bar{n}_e$ by nearly a factor of two (see Fig. 5) the modulation $\Delta\tilde{T}_e(0)$ of the central electron temperature amounts to typically 1oo eV at low, and to 5o eV at high density. The same variation of $T_e(0)$ was measured in the ASDEX device by means of electron cyclotron emission (ECE), which allows direct, continuous measurement of the electron temperature with spatial resolution /17/.

Thus, the location of the sawtooth inversion points, which can be identified with the radius r_1 of the $q = 1$ surface before relaxation, can be obtained from the ECE measurements, whereas it is determined from the soft X-ray method in the case of Pulsator. It is found that in both machines the reduced radius $\rho_1 = r_1/a$ decreases with increasing values of q_a or q'. This behaviour is also described by the profile functions introduced in Section 3 which in the following are supposed to describe the profiles before relaxation. From eq. (2o) it follows that

$$q(\rho) = q(o)\,\frac{q'\,\rho^2}{1-(1-\rho^2)^{q'}} \quad . \tag{44}$$

The current flowing inside the $q = 1$ surface before relaxation is given by

$$I(\rho_1) \equiv I_1 = \rho_1^2\, q_a \cdot I \tag{45}$$

since

$$q' \equiv q_a \,/\, q(o) \quad .$$

From both the Pulsator and the ASDEX data it is seen that the radius r_1 of the sawtooth inversion point amounts to typically 0.3 a at $q_a \sim 4$. This can be described by eq. (44) if $q_o = 3/4$ is chosen. Such low values of the central q do not, however, agree with the present-day understanding of the internal disruption. Owing to the skin effect, the current density inside the q = 1 surface is expected to be far less peaked than $T_e^{3/2}$; the central q value is therefore unlikely to become <0.95 /18/. We thus get a realistic description of the q profile by assuming eq. (44) to be valid at and outside the q=1 surface and q=1 for $0 \leq \rho \leq \rho_1$. If eq. (44) is expanded into a Taylor series, we get in first order with respect to ρ^2

$$\rho_1^2 = \frac{2(q'-q_a)}{q'(q'-1)} \quad . \tag{46}$$

Equation (46) fits the experimental data if

$$q' = q_a + 1$$

is chosen. We thus get

$$\rho_1^2 = \frac{2}{q_a(q_a+1)} \quad . \tag{47}$$

Substituion of this approximation in eq. (45) yields

$$I_1 = \frac{2}{q_a+1} \cdot I \tag{48}$$

which agrees with the assumption of a constant current density $2B_\varphi/\mu_o R$ inside the q=1 surface. In the following, eqs.(47) and (48) will be used to estimate the energy transported through the q=1 surface during an internal disruption.

Before this, we continue discussion of the experimental data. A further common feature of the two machines is the way the sawtooth period $\overset{\frown}{\tau}$ depends on the density, which is very similar to that of the energy confinement time τ_E: $\overset{\frown}{\tau}$ starts to grow linearly with $\bar{n}_e$ but saturates at the same densities at which τ_E does. The saturation levels amount to ~2.5 ms and ~1o ms for Pulsator and ASDEX, respectively. The ratio $\overset{\frown}{\tau}/\tau_E$ is thus approximately constant, being 0.2 - 0.25. This proportionality can be explained as follows: The fraction of the electron energy lost in the internal disruption is practically equal to $\Delta\overset{\frown}{T}_e/T_e$ since $\Delta\overset{\frown}{n}_e/n_e \ll \Delta\overset{\frown}{T}_e/T_e$ which was shown to be independent on density. The lost fraction of the ion energy was not measured but must be supposed to be equal to that of the electron energy, provided that $T_i \sim T_e$; if, on the other hand, $T_i \ll T_e$, the ions can be neglected. This means that the relative loss of total energy does not depend on $\bar{n}_e$ and hence the time needed to regain it must be a constant fraction of the energy confinement time τ_E, which was shown to be independent of the minor radius r.

Thus we get approximately

$$\frac{\Delta(\overset{\frown}{W}_e + \overset{\frown}{W}_i)}{\overset{\frown}{\tau}} \cdot \frac{\tau_E}{W_e + W_i} \sim \frac{\Delta\overset{\frown}{T}_e}{T_e} \cdot \frac{\tau_E}{\overset{\frown}{\tau}}$$

at the centre of the plasma column. Substitution of $\Delta\overset{\frown}{T}_e = 0.1 T_e(0)$ and $\overset{\frown}{\tau} \sim 0.2\ \tau_E$ yields

$$\frac{\partial}{\partial t} n(0)\ T_s(0) = \frac{1}{2}\frac{1}{\tau_E} n(0)\ T_s(0) \qquad (49)$$

in both limiting cases $T_i = T_e$ and $T_i \ll T_e$. This means that 1/3 of the central power density is needed to replace the energy density lost owing to the internal disruption. The fraction becomes smaller if we integrate over the radius up to the q=1 surface. $\Delta k\overset{\frown}{T}_s$ can be assumed to have a parabolic profile; we thus get

$$\int_0^{r_1} \frac{\partial}{\partial t} (nkT_s)\, 2\pi r'\, dr' = \frac{1}{2} \cdot \frac{n(o)\, \Delta k\overset{\frown}{T}_s(o)\, \pi r_1^2}{\overset{\frown}{\tau}} \quad . \tag{5o}$$

This quantity has to be compared with

$$\frac{1}{\tau_E} \int_0^{r_1} \frac{3}{2} nkT_s\, 2\pi r'\, dr' \quad .$$

Since the energy density and the current density have the same profiles, the fraction of the total energy residing inside the q=1 surface is I_1/I. With eq. (48) and

$$\int_0^a nkT_s\, 2\pi r'\, dr' = \frac{\pi a^2}{q'}\, n(o)\, kT_s(o)$$

we get

$$\int_0^{r_1} \frac{3}{2} \cdot \frac{nkT_s}{\tau_E}\, 2\pi r'\, dr' = \frac{3}{2} \cdot \frac{n(o) kT_s(o)}{(q_a+1)\tau_E}\, \pi a^2\, \frac{2}{q_a+1} \quad . \tag{51}$$

Using eq. (47), we find

$$\int_0^{r_1} \frac{\partial}{\partial t} (nkT_S)\, 2\pi r' dr' = \frac{1}{4} \frac{q_a}{q_a+1} \int_0^{r_1} \frac{3}{2} \cdot \frac{nkT_S}{\tau_E}\, 2\pi r' dr' \qquad (52)$$

We thus arrive at the conclusion that the sawtooth relaxations, while playing an important role in the energy balance of the near-centre regions, do not markedly affect the global confinement behaviour. In particular, the relative contribution of the internal disruptions to the energy losses does not vary with the density.

6. INTERPRETATION OF THE RESULTS

This section treats the energy losses through the electron and ion channels. It was stated in Section 2 that charge exchange and radiation are only important in the near-boundary region, whereas they can be neglected at radii $\lesssim 3a/4$. Furthermore, it was shown in Section 3 that the convective losses do not appreciably contribute to the energy balance, which, as a consequence, must be governed by heat conduction. Finally, the energy loss due to the internal disruption was estimated in the preceding section; it was found that only in the very near-centre region are the profiles essentially influenced. The energy balance equations (2) and (3) can thus be reduced to

$$-\frac{1}{r}\frac{\partial}{\partial r}\left(r n_e \chi_e \frac{\partial kT_e}{\partial r}\right) = j(r)\,E - p_{ei}(r) \quad , \tag{2c}$$

$$-\frac{1}{r}\frac{\partial}{\partial r}\left(r n_i \chi_i \frac{\partial kT_i}{\partial r}\right) = p_{ei}(r) \quad . \tag{3c}$$

In principle, the electron heat conductivity

$$\varkappa_e = n_e \chi_e$$

can be determined experimentally according to the equation

$$-2\pi r \varkappa_e \frac{\partial kT_e}{\partial r} = E\,I(r) - P_{ei}(r) \tag{2e}$$

which is obtained by integrating eq. (2c). In doing so, we find that κ_e appears to be independent of density; the error bars, however, are too large to arrive at safe statements on the dependence on other quantities such as T_e, B_φ, Z_{eff} etc. . In particular, at elevated density the errors caused by $T_e(r) - T_i(r)$ which enter into $P_{ei}(r)$ prevent a detailed analysis of the data. It therefore appears more promising to infer the parameter dependence of κ_e or χ_e from that of the energy confinement time τ_{Ee} since it was shown in Section 4 that the Pulsator data obtained at densities $\leq 0.8 \times 10^{14} cm^{-3}$ can be exclusively attributed to electron heat conduction. Due to the "ohmic heating constraint", however, this procedure does not lead to a unique answer. While the argument is well known, we shall repeat it in a simplified fashion: Let us suppose the electron energy confinement time to follow a scaling law of the type

$$\tau_{Ee}^{(S)} = c_S \cdot n_e^{S_n}(0) \cdot T_e^{S_T}(0) \cdot B_a^{S_B}$$

where profile factors are included in c_S. In an ohmically heated plasma the steady-state energy balance without the contribution of the ions yields

$$\tau_{Ee}^{(\Omega)} = c_\Omega \cdot n_e(0) \cdot T_e^{5/2}(0) \cdot B_a^{-2} \quad .$$

One of the three variables, e.g. $T_e(0)$, can thus be expressed by the other two, and there is no way of determining the full parameter dependence of τ_{Ee} in ohmically heated plasmas. Obviously, this constraint no longer holds if other heating or loss processes become important for the energy balance of the electrons. Actually, the power transfer to the ions is such a

mechanism. Unfortunately, under the conditions where it can be determined with sufficient accuracy (low and intermediate densities in Pulsator) it only marginally affects the electron temperatures.

There is, however, more indirect evidence of the way in which the electron heat conductivity depends on T_e: Guest, Miller, Pfeiffer and Waltz have shown /2/ that the ansatz

$$\chi_e(r) = f_o \cdot \frac{I(r)\,(kT_e(r))^p}{r^2\, n_e(r)} \tag{53}$$

leads in the case $p_{ei} = 0$ to a class of analytic solutions of eq.(2e)(p.68) if f_o does not depend on r but is allowed to depend on, for example, B_φ, R, Z_{eff} etc.. This class of solutions reads

$$T_e^{p+1}(\rho) = T_e^{p+1}(o)\,(1-\rho^2) \quad ; \quad \rho = \frac{r}{a} \quad . \tag{54}$$

Here, the central electron temperature $T_e(0)$ is given by

$$\left[kT_e(o)\right]^{p+\frac{5}{2}} = \frac{p+\frac{5}{2}}{4\,\pi^2} \cdot \frac{I}{f_o} \cdot \frac{Z_{eff}}{\sigma^*} \quad , \tag{55}$$

where σ^* is defined by eq. (25). The essential drawback of the ansatz (53) and the consequent solution (54) is the rigid correlation between the exponent p and the profile parameter q'. For $q' = q_a + 1$ we get

$$p = \frac{3}{2\,q_a} - 1 \quad . \tag{56}$$

In the region $2.2 \leq q_a \leq 5.4$ covered by the experiments, p ranges between -0.72 and -0.32.If the electron energy losses are ascribed to heat conductivity, i.e. to local processes, χ_e cannot be allowed to depend on non-local quantities such as q_a. In this connection it should be noted that

$$\frac{I(r)}{r^2} = \frac{2\pi B_\varphi}{\mu_o R \; q(r)}$$

is a local quantity. It might be possible to reconcile the requirements for keeping the exponent constant and for varying q_a by taking into account terms neglected in eq. (2e). It would exceed the scope of this paper, however, to pursue these ideas further. For the present, we choose $q = -1/2$ as the "most plausible exponent" where the error is ±0.25. This leads to

$$kT_e(\rho) = kT_e(o)\,(1-\rho^2)^2 \tag{57}$$

and consequently to $q' = 4$, $q_a = 3$. The parameter dependence of f_o is found by comparing eq. (55) with eq. (39) putting $g(n_{14}) = \text{const}$. This leads to

$$f_o = k_o \, Z_{eff}^{1/3} \frac{R}{B_\varphi}$$

where k_o is a constant and hence to

$$\chi_e = \chi_{eo} \frac{Z_{eff}^{1/3}}{n_{14}(r) \; T_{e1}^{1/2}(r) \; q(r)} \tag{58}$$

where

$$T_{e1} \equiv \frac{kT_e}{1\,keV} \quad .$$

According to eq. (58), χ_e does not depend on B_φ. This result, however, is based on a set of data obtained from experiments in which the toroidal magnetic field was only marginally varied.

The constant k_o can be best obtained by comparing the empirical equation (29) describing the electron energy confinement time obtained in Pulsator with the theoretical relation according to eq. (58). This procedure leads to $\chi_{eo} = 2.7 \times 10^3 cm^2 s^{-1}$.

According to eq. (58), the electron heat diffusion coefficient χ_e increases with minor radius owing to the decrease of the density and electron temperature. Outside the q=1 surface, the decrease is counteracted by the increase of q. With the "standard profiles"

$$\hat{n}_e \equiv \frac{n_e(\rho)}{n_e(o)} = 1 - \rho^2$$

for n_e and eq. (57) for T_e, for example, the reduced radius ρ_1 of the q=1 surface is found to be 0.4. This leads to $\chi_e(0.4) = 1.4\ \chi_e(0)$, $\chi_e(0.7) = 2.4\ \chi_e(0)$.

The ion energy balance in Pulsator was investigated by Wagner /9/. It was shown there that, except at very low densities, heat conduction is the dominant loss mechanism in the near-centre region. Since the ions are in the plateau regime, the χ_i values experimentally found were compared with the Galeev-Sagdeev formula /1/:

$$\chi_i = \chi_{io} \frac{q(r)\ T_{i1}^{3/2}(r)}{R_{100}\ B_{25}^2} \qquad (59)$$

where

$$T_{i1} \equiv \frac{kT_i}{1\,keV} \quad ; \quad R_{100} \equiv \frac{R}{100\,cm} \quad .$$

The constant χ_{io} is $1.9 \times 10^4 cm^2 s^{-1}$. In Ref. /9/ it is shown that these theoretical values must be enhanced by a factor of typically 2 - 4 in order to explain the measured T_i profiles; otherwise the calculated central ion temperatures become somewhat too large. On the other hand, the energy losses due to sawtooth relaxations, not considered in Ref. /9/, might be responsible for the enhancement needed to obtain agreement. Since no experimental data on the modulation of the ion temperature are available, this question must be left open.

According to eq. (59), the ion heat diffusion coefficient χ_i tends to decrease with minor radius. With the profile function

$$\hat{T}_i(\rho) \equiv \frac{T_i(\rho)}{T_i(o)} = (1-\rho^2)^{\Theta_i} \quad ,$$

$\Theta_i = 1.5$ and $q(\rho)$ according to $q' = 4$ we find, for example, $\chi_i(0.4) = 0.7\ \chi_i(0)$, $\chi_i(0.7) = 0.35\ \chi_i(0)$. Hence the ratio $\chi_i(\rho)/\chi_e(\rho)$ decreases from the centre to the boundary owing to both the decrease of χ_i and the increase of χ_e. This radial variation of the ratio χ_i/χ_e agrees with the experimentally found behaviour of the power p_{ei} transferred from the electrons to the ions, as discussed in Section 3.

In the following, an attempt is made to explain the Pulsator and the ASDEX data by assuming eqs.(58) and (59) for χ_e and χ_i to be valid for both machines at all densities. For this

purpose, we add the energy balance equations (2c) and (3c)(p.68), which yields

$$-\frac{1}{r}\frac{\partial}{\partial r}\, r\, n_e\left[\chi_e \frac{\partial kT_e}{\partial r} + \chi_i \frac{\partial kT_i}{\partial r}\right] = j(r)\cdot E \quad ,$$

where, for the sake of simplification, $n_i = n_e$ is assumed. We use

$$\hat{T}_e(\rho) = \frac{T_e(\rho)}{T_e(o)}$$

and insert eqs. (58) and (59) for χ_e and χ_i. This leads to

$$-\frac{1}{\rho}\frac{\partial}{\partial \rho}\,\rho\cdot\left[\frac{\chi_{eo}\, Z_{eff}^{1/3}\, T_{e1}^{1/2}(o)}{q(\rho)}\cdot 2\cdot\frac{\partial \hat{T}_e^{1/2}}{\partial \rho} + \frac{\chi_{io}\, T_{i1}^{5/2}(o)\; q(\rho)\; n_{14}(\rho)}{R_{100}\, B_{25}^2}\cdot\frac{5}{2}\cdot\frac{\partial \hat{T}_i^{5/2}}{\partial \rho}\right] =$$

$$= \lambda\left(\frac{B_{25}}{A_5\, q(o)}\right)^2 Z_{eff}\;\frac{\hat{T}_e^{3/2}(\rho)}{T_{e;}^{3/2}(o)} \qquad (60)$$

where the constant λ is $0.94 \times 10^4 \mathrm{cm}^2\mathrm{s}^{-1}$. From this equation it follows that the central electron and ion temperatures are both proportional to B_φ, as can easily be seen if eq. (60) is divided by $B_{25}^{1/2}$. In Section 4 the sum $T_s = T_e + T_i$ of the temperatures was shown to be proportional to the toroidal magnetic field in both Pulsator an ASDEX. This parameter dependence agrees with eq. (60).

In order to discuss the contributions of the electrons and the ions to the heat flow through a surface with the reduced

radius ρ, we integrate eq. (6o) after multiplication by 2 ρ and get

$$\chi_{eo} Z_{eff}^{1/3} T_{e1}^{1/2}(o)\left(-\frac{4\rho}{q(o)} \frac{\partial \hat{T}_e^{1/2}}{\partial \rho}\right) + \frac{\chi_{io} n_{14}(o) T_{i1}^{5/2}(o)}{R_{100} B_{25}^2}\left(-\frac{4}{5} \rho q(\rho) \hat{n}_{14}(\rho) \frac{\partial \hat{T}_i^{5/2}}{\partial \rho}\right) = \tag{61}$$

$$= \lambda \left(\frac{B_{25}}{A_5 q(o)}\right)^2 \frac{Z_{eff}}{T_{e1}^{3/2}(o)} \int_o^\rho \hat{T}_e^{3/2} d\rho'^2 \quad .$$

With the usual profile functions we obtain

$$\frac{4\rho}{q(\rho)} \cdot \frac{\partial \hat{T}_e^{1/2}}{\partial \rho} \equiv \rho^2 \cdot g_e(\rho) = \rho^2 \cdot \frac{4\Theta_e}{q(\rho)} (1-\rho^2)^{\frac{\Theta_e}{2}-1} \quad , \tag{62a}$$

$$-\frac{4}{5} \rho q(\rho) \hat{n}_{14}(\rho) \frac{\partial \hat{T}_i^{5/2}}{\partial \rho} \equiv \rho^2 g_i(\rho) = \rho^2 4 \Theta_i q(\rho) (1-\rho^2)^{\frac{5\Theta_i}{2}+\nu-1} \quad , \tag{62b}$$

$$\int_o^\rho \hat{T}_e^{3/2} d\rho'^2 = \frac{1-(1-\rho^2)^{q'}}{q'} = \rho^2 \frac{q(o)}{q(\rho)} \quad , \tag{62c}$$

which leads to

$$\rho^2 g_e(\rho) \chi_{eo} Z_{eff}^{1/3} T_{e1}^{1/2}(o) + \rho^2 g_i(\rho) \chi_{io} \frac{n_{14}(o)}{R_{100} B_{25}^2} T_{i1}^{5/2}(o) = \tag{63}$$

$$= \frac{\rho^2}{q(\rho)} \frac{\lambda}{q(o)} \left(\frac{B_{25}}{A_5}\right)^2 \frac{Z_{eff}}{T_{e1}^{3/2}(o)} \quad .$$

Further discussion of the confinement behaviour will be based on this equation. Our main concern is the study of the ratio of the terms on the left-hand side of eq.(63), namely

$$\gamma_p(\rho) = \frac{n_{14}(o)\,\chi_{io}\,T_{i1}^{5/2}(o)}{\chi_{eo}\,Z_{eff}^{1/3}\,T_{e1}^{1/2}(o)\,R_{100}\,B_{25}^{2}} \quad \frac{g_i(\rho)}{g_e(\rho)} \tag{64}$$

which can be separated into the study of the profile-dependent functions g_i and g_e and the study of the central temperatures $T_i(0)$ and $T_e(0)$.

Let us start with the discussion of g_i and g_e for typical profiles, i.e. typical values of the exponents. As for Θ_e and ν, we use the standard values 2 and 1, respectively. In the case of ASDEX, Θ_i ranges typically between 1.4 and 1.8; this also holds for the Pulsator profiles at the highest densities at which T_i approaches T_e at all radii. For the following calculations $\Theta_i = 1.6$ is thus chosen, and we discuss

$$\rho^2\, g_e(\rho) = 8\,\frac{\rho^2}{q(\rho)} \quad ,$$

$$\rho^2\, g_i(\rho) = 6.4\;\rho^2\; q(\rho)\,(1-\rho^2)^4 \quad .$$

These two functions and the ratio g_i/g_e are plotted in Fig. 41. According to the considerations presented in Section 5, we put $q = 1$ for $\rho \leq \rho_1 = 0.408$ and calculate $q(\rho)$ according to eq. (44) for $\rho \geq \rho_1$. Obviously, the profile functions are insignificant near $\rho = 1$ because the gradients become zero or singular unless the profile is a parabola. This problem could be circumvented by introducing an extrapolated radius; the profile functions, however, are not aimed at modelling density and temperatures in

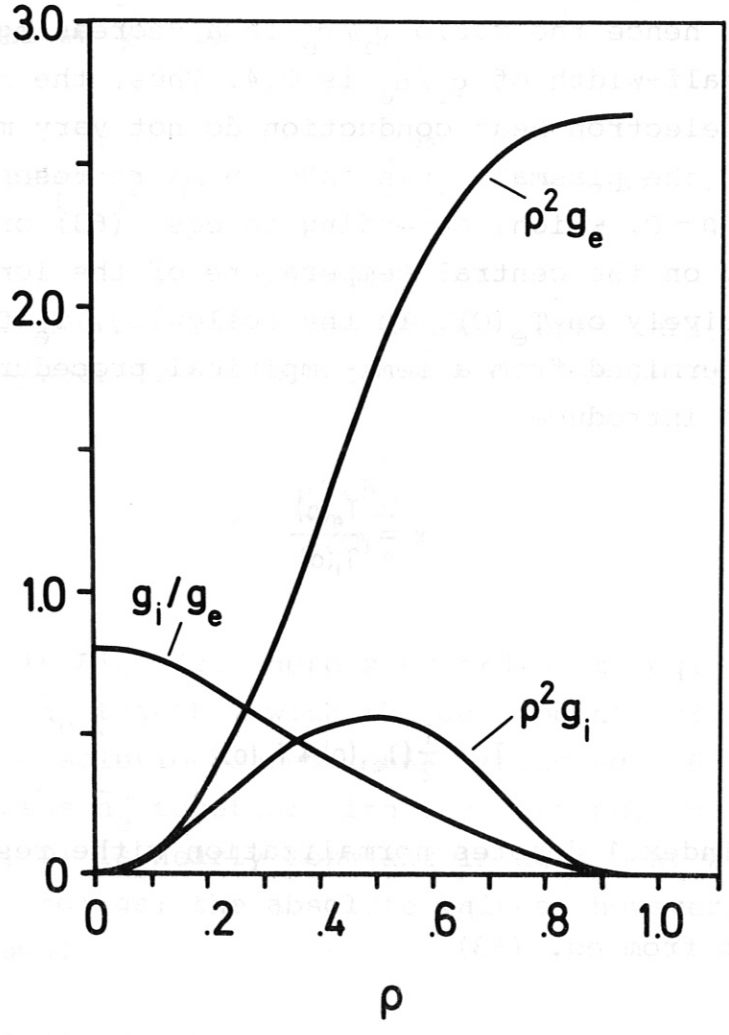

Fig.41: The profile factors $\rho^2 g_e$ and $\rho^2 g_i$ describe the radial variation of the electron and ion heat losses, respectively, according to eqs.(62a,b).

the outer zones, where there are no measured values. It is sufficient if they describe the data at radii ≤ 0.8 a.

According to Fig.41, $\rho^2 g_e$ rises monotonically up to the boundary of the plasma column, whereas $\rho^2 g_i$ has a maximum near $\rho = 0.5$; hence the ratio g_i/g_e is a decreasing function of ρ. The half-width of g_i/g_e is 0.4. Thus, the relative roles of ion and electron heat conduction do not vary markedly in the core of the plasma column and can be represented by the values at $\rho = 0$, which, according to eqs. (63) or (64), depend sensitively on the central temperature of the ions and far less sensitively on $T_e(0)$. In the following, $T_e(0)$ and $T_i(0)$ will be determined from a semi-empirical procedure. For this purpose, we introduce

$$x = \frac{T_e(o)}{T_i(o)}$$

and

$$T_1 = \frac{1}{2}(T_{e1}(o) + T_{i1}(o))$$

where the index 1 denotes normalization withe respect to 1 keV.

We thus get from eq. (63)

$$\frac{32x^2}{(1+x)^2} X_{eo} Z_{eff}^{1/3} T_1^2 + \frac{102.4\, x^{3/2}}{(1+x)^4} X_{io} \frac{n_{14}(o)}{R_{100} B_{25}^2} \cdot T_1^4 = \lambda \left(\frac{B_{25}}{A_5}\right)^2 Z_{eff} \quad . \qquad (65)$$

The solutions of this equation can be compared with the reduced data $kT_s^{**}(0)/2$, which are plotted versus $\bar{n}_e$ in Figs. 37 and 38 for Pulsator and ASDEX, respectively. We thus choose $B_\varphi = 27$ kG, $Z_{eff} = 2$ for Pulsator, $B_\varphi = 22$ kG, $Z_{eff} = 1.15$ for ASDEX; in addition, we put $n_{14}(0) = 1.5\ \bar{n}_{14}$. With these data we get for Pulsator

$$10.9 \frac{x^2}{(1+x)^2} T_1^2 + 357 \bar{n}_{14} \frac{x^{3/2}}{(1+x)^4} T_1^4 = 1.36 \quad . \tag{66}$$

The ratio x of the central temperatures appreciably varies with $\bar{n}_e$, as is seen from Fig. 7. The data can be fitted by

$$x = \frac{0.7 + \bar{n}_{14}}{1.2\ \bar{n}_{14}} \tag{67}$$

This is shown in Fig. 42, where x according to eq. (67) is plotted versus $\bar{n}_e$ together with the data points of Fig. 7. In Fig. 43, the solution of eq. (66), using eq. (67) for x, is plotted versus $\bar{n}_e$ together with the data points of Fig. 37. Apparently, $T_1(0)$ is nearly constant in agreement with the experimental findings; the absolute values, however, are somewhat too small.

In the case of ASDEX, the ratio x is practically independent on $\bar{n}_e$ and can be put equal to 1.2 (see Fig. 8). Thus we get

$$2.70\ T_1^2 + 12.8\ \bar{n}_{14}\ T_1^4 = 1.23 \quad . \tag{68}$$

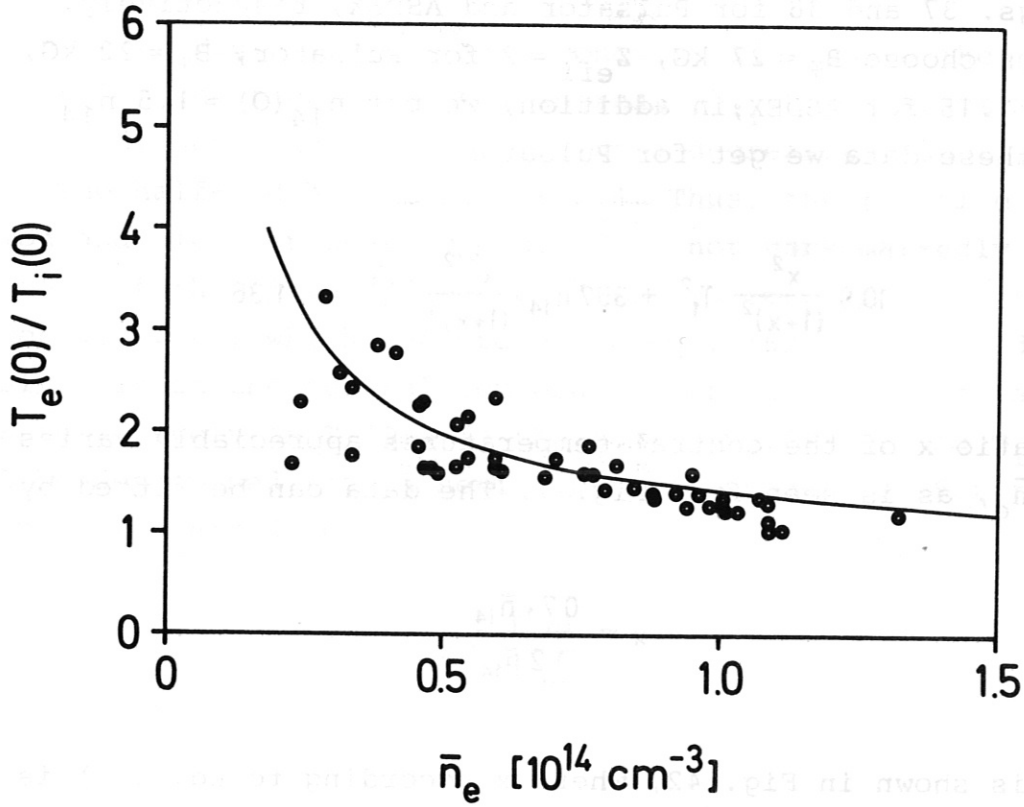

Fig.42: Pulsator.
The measured ratio of the central temperatures (same data points as those of Fig.7) is compared with that calculated according to eq. (67).

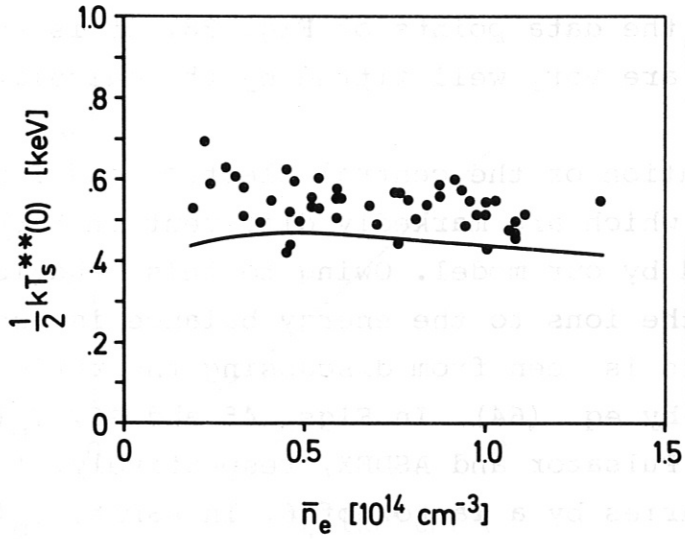

Fig.43: Pulsator.
The quantity $\frac{1}{2}$ k $(T_e(0)+T_i(0)$ is "normalized" to $B_\varphi = 27$ kG, $Z_{eff} = 2$ according to eq.(42). The data points (same as those of Fig.37) are compared with the solution of eq. (66) using the ratio $T_e(0)/T_i(0)$ as shown in Fig.42.

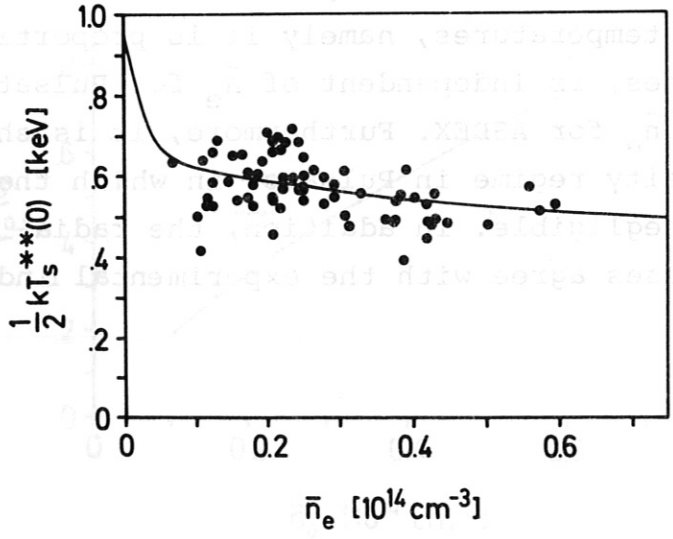

Fig.44: ASDEX.
The quantity $\frac{1}{2}$ k $(T_e(0)+T_i(0)$ is "normalized" to $B_\varphi = 22$ kG, $Z_{eff} = 1.15$ according to eq.(42). The data points (same as those of Fig.38) are compared with the solution of eq.(68).

In Fig. 44, the solution of this equation is plotted versus $\bar{n}_e$ together with the data points of Fig. 38. It is seen that the measured data are very well fitted by the calculated curve.

Thus the variation of the central electron and ion temperatures with density, which are markedly different in both devices, is well described by our model. Owing to this behaviour the contribution of the ions to the energy balance is essentially different. This is seen from discussing the ratio $\gamma_p(0)$ where γ_p is defined by eq. (64). In Figs. 45 and 46, $\gamma_p(0)$ is plotted versus $\bar{n}_e$ for Pulsator and ASDEX, respectively. In both machines the density varies by a factor of 6. In ASDEX, $\gamma_p(0)$ only varies by a factor of 4.1 from $n_{14} = 0.1$ to 0.6. This is due to the decrease of $T_i(0)$. For Pulsator we find $\gamma_p(0) = 0.03$ at $\bar{n}_{14} = 0.2$, $\gamma_p(0) = 1.15$ at $\bar{n}_{14} = 1.2$, which corresponds to a variation of 38 owing to the strong change of $T_i^{5/2}(0)/T_e^{1/2}(0)$.

Hence our model, which is based on neoclassical heat conduction for the ions and anomalous heat conduction according to eq. (58) for the electrons, is able to explain the behaviour of the sum of the central temperatures, namely it is proportional to B_φ for both machines, is independent of $\bar{n}_e$ for Pulsator, and decreases with $\bar{n}_e$ for ASDEX. Furthermore, it is shown that there is a density regime in Pulsator in which the ion heat conduction is negligible. In addition, the radial variation of the heat losses agree with the experimental findings.

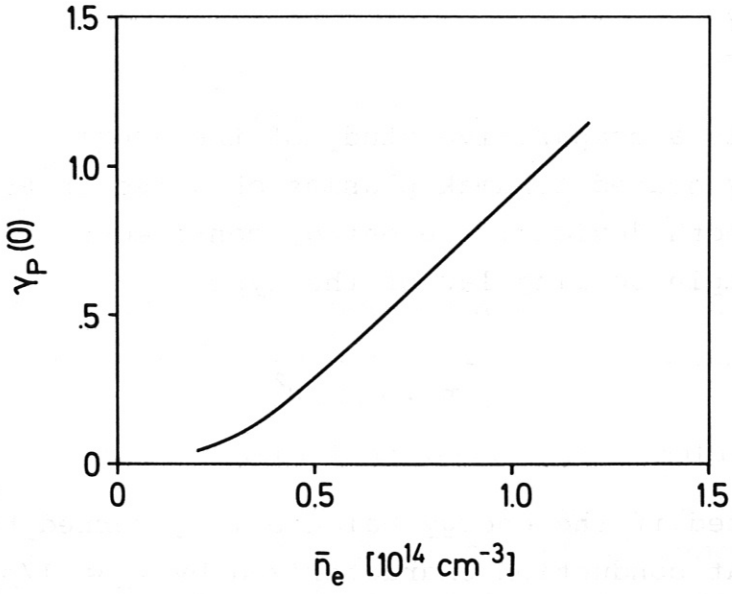

Fig.45: Pulsator.
The ratio of the ion to the electron heat condution losses versus $\bar{n}_e$.

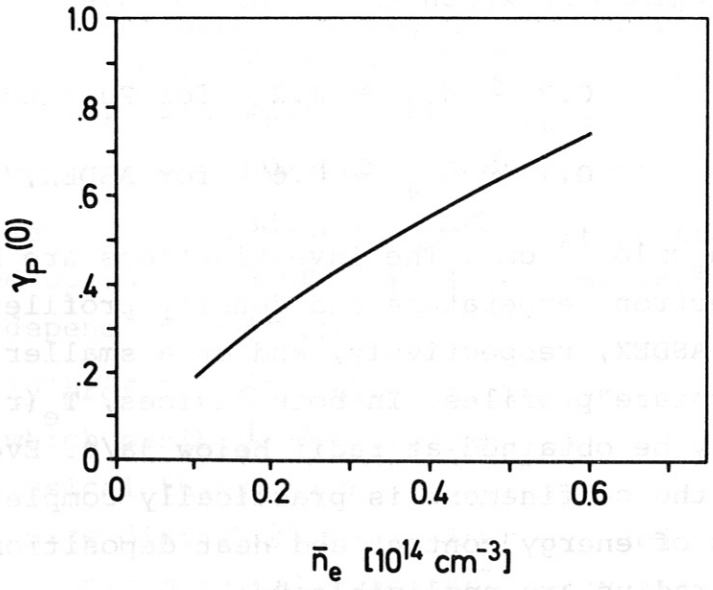

Fig.46: ASDEX.
The ratio of the ion to the electron heat conduction losses versus $\bar{n}_e$.

7. SUMMARY

This paper is a comparative study of the energy confinement of ohmically heated tokamak plasmas obtained in Pulsator and ASDEX. For both devices, the energy confinement time does not follow a simple scaling law of the type

$$\tau_E = c_n \bar{n}_e a^2$$

as is expected if the energy balance is governed by anomalous electron heat conduction characterized by $\chi_e \propto 1/n_e$. It was thus investigated whether or not the deviations could be ascribed to competing loss mechanisms, namely radiation, charge exchange, convection and ion heat conduction, of which the latter - owing to its parameter dependence - appears to be the favourite candidate.

The density regimes in which the machines have been operated are:

$$0.2 \leq \bar{n}_{14} \leq 1.2 \quad \text{for Pulsator,}$$

$$0.1 \leq \bar{n}_{14} \leq 0.6 \quad \text{for ASDEX,}$$

where $\bar{n}_{14} \equiv \bar{n}_e \times 10^{-14}$ cm^3. The investigations are based on 47 and 70 electron temperature and density profiles for Pulsator and ASDEX, respectively, and on a smaller number of ion temperature profiles. In both devices, $T_e(r)$ and $n_e(r)$ can only be obtained at radii below 3a/4. Even so, knowledge of the confinement is practically complete since the fractions of energy content and heat deposition located outside this radius are negligible.

The investigations presented in this paper are restricted to experimental conditions under which the radiation losses from the inner region characterized by $r \leq 3a/4$ can be neglected. The same holds for charge exchange. Only convection and heat conduction thus have to be considered.

The most significant difference between both devices is the way the particle-averaged temperatures depend on density. In Pulsator, T_e decreases and T_i increases with n_e so that the sum $T_e + T_i$ stays constant in good approximation. In ASDEX, both T_e and T_i decrease with density as $n_e^{-1/6}$. The same relations hold approximately for the central temperatures, too. It is discussed to what extent these temperatures are modified by the sawtooth relaxations, which are shown to contribute little to the energy losses outside the q=1 surface.

The study of the profiles has shown that the energy density $n_e(r)k\ (T_e(r) + T_i(r))$ is proportional to $T_e^{3/2}(r)$ and hence to the current density, provided that Z_{eff} does not depend on the radius. (In the ASDEX device, discharges with $Z_{eff} < 1.3$ can be obtained; at least for these plasmas, the current density distribution cannot deviate markedly from $T_e^{3/2}$.) This relation has two substantial consequences:

- The local energy confinement time, i.e. the energy density integrated up to some radius r divided by the power input, does not depend on the radius.
- The density profile is coupled to the temperature profiles in a way which exhibits some resemblance to the Nernst effect of the classical theory. From the profile characteristics and the source distributions it is concluded that convection contributes only marginally to the energy transport. Hence the energy balance is governed by heat conduction.

The profiles of the ion temperature are found to be substantially broader than those of the electrons so that T_i exceeds T_e at larger radii. Hence the power which in the central region is transferred from the electrons to the ions is redeposited in the electrons in the outer zones of the plasma column rather than transported by the ions through the boundary. The analysis of the data has shown that the role of the ions can be neglected in the case of Pulsator at densities below $0.8 \times 10^{14} cm^{-3}$. In this regime, the energy confinement time of the electrons is porportional to $\bar{n}_e$, which indicates a $1/n_e$ dependence of the heat diffusion coefficient χ_e. Owing to the "ohmic heating constraint", the dependence on other parameters cannot be uniquely determined; hence we start from an ansatz which yields a class of analytical solutions of the electron energy balance equation and compare it with the experimental data. This leads to the expression

$$\chi_e \propto \frac{Z_{eff}^{1/3}}{n_e(r)\ T_e^{1/2}(r)\ q(r)}$$

which does not contain the toroidal magnetic field. This might be due to the small variation of B_φ. The error of the exponent of T_e is estimated to be $\pm 1/4$.

Since the ions are in the plateau regime,

$$\chi_i \propto \frac{q(r)\ T_i^{3/2}(r)}{R\ B_\varphi^2}$$

is taken as a basis. Starting from these expressions for χ_e and χ_i, model calculations are performed which explain the following experimental findings:

- the proportionality of the central temperatures $T_e(0)$ and $T_i(0)$ to the toroidal magnetic field,

- the approximate constancy of $T_e(0) + T_i(0)$ in the case of Pulsator,

- the decrease of this quantity with n_e in the case of ASDEX,

- the radial decrease of the ion heat conduction losses and the radial increase of the electron losses.

ACKNOWLEDGEMENT

This paper has benefitted from the work of the entire Pulsator and ASDEX teams. The data are mainly based on Thomson scattering (D.Meisel, H.Murmann), charge exchange analysis (H.M.Mayer, F.Wagner) and interferometry (O.Gehre, G.Lisitano); the authors are particularly indebted to the colleagues involved in these diagnostics. Completion of the work was made possible by the patience and help of E.Reimann (programming), H.Volkenandt (drawing) and S.Beutler (typing).

REFERENCES

/1/ A.A.Galeev,R.Z.Sagdeev, Soviet Physics, JETP 26 233 (1968)

/2/ G.E.Guest, R.L.Miller, W.W.Pfeiffer and R.E.Waltz, GA-A 14831 (1978)

/3/ M.Keilhacker et al., Proc.8th Int.Conf.on Plasma Physics, Brussels 198o, Vol.II, IAEA-CN-38-O1, 351

/4/ E.R.Müller, K.Behringer, H.Niedermeyer, IPP Report III/74 (1981)

/5/ W.Engelhardt, O.Klüber et al., Proc.7th Int.Conf.on Plasma Physics, Innsbruck 1978, IAEA-CN-37-A-5

/6/ W.Engelhardt, S.Sesnic et al., Proc.9th Europ.Conf.on Contr.Fus. D2.1,88 (Oxford 1979)

/7/ D.Meisel et al., Proc.6th Int.Conf.on Plasma Physics, Berchtesgaden 1976, IAEA-CN-35-A-6

/8/ E.R.Müller, private communication

/9/ F.Wagner, IPP Report III/52 (1979)

/1o/ F.Wagner, private communication

/11/ D.Meisel, H.Murmann, to be published

/12/ S.I.Braginskii, Reviews of Plasma Physics (Ed.M.A.Leontovich) Vol.I, Consultants Bureau, New York (1965)

/13/ P.H.Grassmann, O.Klüber, H.Wulff, Phys.Lett.24A, 6, 324 (1967)

/14/ O.Klüber, Z.Naturf.,22a 1o, 1599 (1967)

/15/ A.Gondhalekar et al., Proc.7th Int.Conf.on Plasma Physics, Innsbruck 1978, IAEA-CN-37/C-4

/16/ S.Fairfax, A.Gondhalekar et al., Proc.8th Int.Conf.on Plasma Physics, Brussels 198o, IAEA-CN-38/N-6

/17/ A.Eberhagen, D.Campbell, private communication

/18/ O.Gruber, private communication

APPENDIX

Table 2 PULSATOR Data

B_φ	I	U	$n_e(o)$	$\bar{n}_e$	$T_e(o)$	$\langle T_e \rangle$	$T_i(o)$	Z_{eff}	q	τ_{Ee}	τ_E
[kG]	[kA]	[V]	[10^{13} cm^{-3}]		[keV]		[keV]			[ms]	
29.00	67.00	2.01	14.73	9.20	0.58	0.19	0.42	1.11	3.74	5.54	10.40
29.00	67.00	2.30	18.36	10.03	0.56	0.19	0.42	1.39	3.74	5.35	9.15
28.80	67.80	2.51	13.74	9.37	0.55	0.17	0.44	1.21	3.67	4.13	7.92
28.40	63.60	2.73	15.33	10.28	0.51	0.16	0.43	1.34	3.86	4.21	8.00
28.00	46.60	2.91	16.78	11.09	0.45	0.13	0.44	1.70	5.19	5.16	9.76
27.80	61.00	2.20	6.69	4.66	0.60	0.22	0.26	2.16	3.94	3.64	5.51
27.80	58.50	2.88	11.36	7.64	0.58	0.19	0.31	2.42	4.11	4.08	6.48
27.80	53.50	2.53	15.96	10.07	0.45	0.19	0.37	2.12	4.49	6.11	10.70
28.00	37.50	3.28	7.17	4.57	0.63	0.21	0.35	4.41	5.33	2.75	3.78
28.00	57.20	2.70	15.64	9.78	0.53	0.17	0.42	1.81	4.23	4.72	8.52
27.60	63.00	1.98	8.85	6.07	0.62	0.22	0.39	1.65	3.79	4.73	8.06
27.90	62.50	2.08	6.05	3.40	0.63	0.22	0.26	1.48	3.86	2.21	3.16
28.00	57.00	2.41	8.41	4.94	0.60	0.23	0.38	2.22	4.25	3.13	4.94
27.80	57.90	2.85	13.60	10.85	0.48	0.22	0.43	1.98	3.43	4.72	8.62
27.80	57.90	2.86	13.87	10.85	0.44	0.19	0.43	1.60	3.43	4.22	8.00
27.60	52.00	2.43	12.94	8.14	0.58	0.19	0.35	2.08	4.59	5.25	8.64
27.60	45.30	3.09	17.99	10.65	0.47	0.15	0.35	1.62	4.35	3.93	7.11
26.60	54.70	1.80	4.66	2.93	0.81	0.22	0.24	1.57	4.20	2.69	3.91
27.00	54.00	1.90	7.92	5.26	0.69	0.24	0.34	2.09	4.32	5.06	7.92
27.00	53.00	2.25	10.70	7.05	0.57	0.22	0.34	2.16	4.40	5.17	8.54
27.60	48.00	2.79	15.18	9.49	0.54	0.16	0.34	2.03	4.97	4.92	8.43
27.40	56.00	2.79	14.30	9.62	0.59	0.18	0.43	2.03	4.23	4.79	8.53
27.40	54.50	2.98	15.18	10.03	0.53	0.17	0.43	2.04	4.35	4.44	7.96
27.40	57.00	2.38	11.47	7.57	0.66	0.19	0.42	2.11	4.15	5.02	8.45
27.40	55.70	2.51	12.55	7.92	0.63	0.19	0.44	2.27	4.25	5.04	8.43
27.40	54.50	2.52	13.60	8.44	0.64	0.21	0.45	2.64	4.35	5.69	9.33
27.00	85.50	2.46	14.44	10.85	0.57	0.25	0.45	2.00	2.73	5.93	10.10
27.40	89.00	2.70	19.11	13.20	0.54	0.20	0.45	1.29	2.66	4.85	9.19
27.00	59.50	2.10	9.39	5.94	0.65	0.21	0.40	1.85	3.92	4.61	7.71
27.20	58.00	2.27	11.70	7.71	0.67	0.24	0.43	2.30	4.05	5.54	9.39
27.40	56.00	2.45	12.55	8.78	0.61	0.20	0.46	2.16	4.23	5.78	10.30
27.40	54.50	2.51	14.01	8.78	0.61	0.17	0.45	1.87	4.35	5.12	9.12
27.40	60.00	1.85	5.47	3.16	0.82	0.26	0.32	1.97	3.95	3.07	4.68
27.60	56.50	2.15	9.58	4.57	0.85	0.24	0.38	2.31	4.22	3.70	5.78
27.60	54.00	2.20	10.91	5.49	0.69	0.19	0.40	1.90	4.42	3.96	6.63
27.00	72.00	2.01	3.06	1.97	0.88	0.28	0.18	2.12	3.24	1.55	2.00
27.00	77.50	2.20	5.64	3.87	0.80	0.32	0.28	2.64	3.01	3.04	4.18
27.00	81.00	2.23	8.25	5.94	0.63	0.27	0.37	1.91	2.88	3.79	6.13
27.00	56.50	2.30	5.70	3.40	0.69	0.21	0.39	2.06	4.13	2.37	3.79
27.00	55.50	2.45	7.61	4.68	0.63	0.21	0.39	2.41	4.20	3.18	4.97
27.00	54.00	2.73	9.12	5.26	0.64	0.19	0.39	2.38	4.32	2.95	4.70
20.00	41.00	2.12	3.67	2.45	0.47	0.14	0.21	1.22	4.22	1.63	2.66
20.00	42.50	2.30	6.55	4.80	0.45	0.14	0.28	1.40	4.07	3.05	5.41
20.00	42.00	2.60	10.38	6.83	0.44	0.15	0.28	1.94	4.12	4.15	7.07
22.60	67.00	1.56	3.22	2.31	0.59	0.24	0.35	1.04	2.92	2.11	3.78
22.40	72.00	2.16	7.32	5.49	0.53	0.21	0.25	1.32	2.69	3.20	5.15
27.50	57.00	1.83	9.03	5.94	0.58	0.17	0.25	1.02	4.17	4.27	6.91
27.13	58.00	1.83	6.55	4.16	0.69	0.22	0.25	1.53	4.04	3.60	5.21

Table 3 ASDEX Data

B_φ	I	U	$n_e(o)$	$\bar{n}_e$	$T_e(o)$	$\langle T_e \rangle$	$T_i(o)$	Z_{eff}	q	τ_{Ee}	τ_E
[kG]	[kA]	[V]	[10^{13}	cm^{-3}]	[keV]		[keV]			[ms]	
22.00	230.00	1.30	1.87	1.27	1.03	0.36	0.70	3.66	4.65	19.48	30.30
22.00	267.00	1.70	1.87	1.27	0.87	0.33	0.71	3.56	3.99	11.62	18.70
22.00	248.00	1.90	1.73	1.18	0.94	0.35	0.69	5.53	4.29	11.72	15.50
22.00	244.00	1.90	1.87	1.27	0.85	0.34	0.70	4.91	4.38	11.76	16.90
22.00	286.00	1.50	2.18	1.48	0.89	0.36	0.69	3.35	3.73	15.89	25.50
22.00	258.00	1.20	3.35	2.27	0.74	0.28	0.74	1.90	4.14	27.33	51.00
22.00	253.00	1.10	3.46	2.36	0.79	0.27	0.69	1.63	4.22	30.87	57.60
22.00	253.00	1.20	3.25	2.21	0.72	0.25	0.65	1.68	4.22	25.25	47.00
22.00	253.00	1.25	3.19	2.18	0.76	0.25	0.68	1.67	4.22	23.13	43.30
22.00	258.00	1.20	3.10	2.10	0.76	0.26	0.69	1.74	4.14	24.29	45.30
22.00	247.00	1.00	3.49	2.02	0.71	0.26	0.69	1.48	4.32	28.30	50.80
22.00	259.00	1.84	1.81	1.09	0.63	0.27	0.48	3.48	4.12	8.70	12.30
22.00	256.00	1.65	1.67	1.05	0.85	0.31	0.54	3.91	4.17	11.23	15.70
22.00	258.00	1.05	1.88	1.19	0.72	0.33	0.58	2.49	4.14	20.76	31.40
22.00	248.00	0.94	1.01	0.70	0.91	0.33	0.56	2.40	4.31	15.29	23.60
22.00	246.00	1.00	2.72	1.61	0.57	0.28	0.51	1.52	4.33	22.70	37.50
22.00	253.00	1.10	2.97	1.82	0.59	0.27	0.46	1.48	4.21	22.75	37.60
22.00	253.00	1.23	3.53	2.20	0.55	0.26	0.51	1.61	4.21	23.28	41.50
22.00	253.00	1.05	3.63	2.10	0.61	0.40	0.48	2.56	4.21	31.89	45.80
22.00	252.00	1.20	3.86	2.24	0.67	0.28	0.55	1.85	4.23	26.41	44.00
22.00	253.00	1.45	5.81	3.29	0.63	0.20	0.45	1.36	4.21	23.26	39.90
22.00	255.00	1.35	6.55	3.64	0.55	0.19	0.33	1.07	4.17	24.68	40.40
22.00	305.00	1.45	7.61	4.34	0.55	0.21	0.39	1.13	3.50	25.29	41.60
22.00	305.00	1.45	7.69	4.48	0.49	0.19	0.39	1.00	3.50	23.65	41.50
22.00	252.00	1.50	2.77	1.82	0.76	0.30	0.74	3.31	4.23	20.31	33.20
22.00	258.00	1.20	3.35	2.10	0.61	0.29	0.53	1.68	4.14	22.25	40.10
22.00	258.00	1.20	3.53	2.45	0.60	0.23	0.47	1.22	4.14	23.12	43.30
22.00	253.00	1.50	5.37	3.88	0.48	0.19	0.26	1.25	4.21	24.67	41.20
22.00	253.00	1.56	5.99	4.20	0.41	0.17	0.38	1.03	4.21	22.79	43.70
22.00	248.00	1.56	5.87	4.27	0.44	0.17	0.41	1.06	4.29	24.06	47.00
22.00	246.00	1.56	5.75	4.31	0.44	0.17	0.42	1.04	4.33	24.42	48.10
22.00	246.00	1.56	5.81	4.31	0.52	0.18	0.50	1.16	4.33	25.83	50.60
22.00	253.00	1.56	6.30	4.21	0.45	0.18	0.43	1.11	4.22	25.38	49.80
22.00	248.00	1.56	6.05	4.03	0.52	0.19	0.50	1.26	4.30	26.10	50.90
22.00	246.00	1.56	5.53	3.75	0.45	0.18	0.43	1.15	4.33	23.44	46.00
22.00	253.00	1.56	4.44	3.08	0.58	0.24	0.50	1.87	4.21	22.71	41.20
22.00	243.00	1.20	3.56	2.66	0.62	0.23	0.56	1.39	4.38	24.05	45.70
22.00	243.00	1.20	3.97	2.52	0.67	0.27	0.50	1.75	4.38	28.35	50.10
22.00	248.00	1.20	2.83	1.75	0.72	0.32	0.58	2.53	4.30	23.71	38.80
22.00	248.00	1.30	3.46	2.10	0.66	0.28	0.54	2.14	4.30	22.52	37.20
22.00	244.00	1.80	3.78	2.52	0.60	0.21	0.56	1.90	4.37	14.91	27.60
22.00	244.00	1.50	4.26	2.94	0.55	0.20	0.50	1.34	4.37	20.04	38.30
22.00	246.00	1.40	4.57	2.94	0.62	0.22	0.51	1.41	4.34	22.98	43.20
22.00	244.00	1.35	3.94	2.24	0.65	0.26	0.61	1.84	4.37	20.62	37.90
22.00	244.00	1.25	3.06	1.89	0.68	0.28	0.64	1.97	4.37	21.00	38.70
22.00	241.00	1.25	2.60	1.54	0.85	0.32	0.68	2.53	4.43	19.41	33.70
22.00	239.00	1.20	1.85	1.12	0.82	0.33	0.70	2.58	4.46	15.76	27.10
22.00	244.00	2.10	4.57	3.15	0.61	0.19	0.48	2.29	4.37	15.83	27.70
22.00	234.00	1.20	5.00	3.08	0.69	0.22	0.48	1.41	4.56	31.20	55.50
22.00	241.00	1.40	4.53	2.80	0.68	0.23	0.43	1.76	4.43	24.77	43.30
22.00	241.00	1.30	3.35	1.96	0.73	0.25	0.62	1.84	4.43	19.95	36.00
22.00	241.00	1.30	2.83	1.75	0.79	0.28	0.59	2.27	4.43	19.85	34.30
22.00	243.00	1.40	3.86	2.52	0.71	0.24	0.55	1.84	4.39	23.05	41.30
18.50	412.00	1.40	3.35	2.45	0.74	0.31	0.61	1.50	2.18	17.15	32.00
18.50	412.00	1.45	3.53	2.52	0.75	0.34	0.60	1.78	2.18	18.38	32.90
22.00	234.00	0.95	2.25	1.33	0.64	0.25	0.57	1.09	4.56	18.16	35.40
22.00	234.00	1.00	3.71	2.38	0.51	0.21	0.51	1.00	4.56	27.64	55.10
22.00	234.00	1.00	3.35	2.10	0.56	0.23	0.56	1.00	4.56	24.84	49.20
22.00	234.00	1.00	2.65	1.68	0.56	0.20	0.56	1.00	4.56	18.79	37.70
22.00	230.00	1.40	5.87	3.92	0.53	0.18	0.52	1.01	4.64	26.92	53.20
22.00	234.00	1.85	8.58	5.95	0.46	0.13	0.45	1.00	4.56	26.65	52.80
22.00	234.00	1.80	8.50	5.74	0.45	0.12	0.43	1.00	4.56	23.90	48.10
22.00	234.00	1.60	6.36	4.20	0.48	0.17	0.46	1.11	4.56	24.73	48.50
22.00	234.00	1.10	3.82	2.52	0.52	0.19	0.46	1.00	4.56	24.31	48.10
22.00	234.00	1.75	7.54	5.04	0.42	0.13	0.40	1.00	4.56	22.58	45.20
22.00	234.00	1.75	8.08	5.60	0.50	0.13	0.48	1.00	4.56	26.05	51.60
22.00	234.00	1.35	6.23	3.78	0.46	0.20	0.44	1.21	4.55	29.29	55.30
22.00	237.00	1.20	5.87	3.78	0.50	0.22	0.48	1.19	4.51	35.17	68.20
22.00	237.00	1.30	5.58	3.85	0.49	0.19	0.47	1.02	4.51	30.48	60.10
22.00	239.00	1.10	5.10	2.80	0.57	0.24	0.55	1.30	4.46	31.46	56.20